Check for updates

JGR Oceans

RESEARCH ARTICLE

10.1029/2021JC017373

Special Section:
Significant advances in ocean and climate sciences of the Pacific-Asian Marginal Seas

Key Points:
- Coastal radar data and long-term multisatellite data are used to observe the formation of oceanic fronts driven by ocean currents
- The Kuroshio Current's intrusion of the shelf causes the Northern Taiwan Coastal Current to flow southward along western Taiwan in winter
- Virtual drifter experiments present the possible trajectories of and seasonal changes in near-surface ocean currents

Correspondence to:
R.-S. Tseng,
rstseng@mail.nsysu.edu.tw

Citation:
Hsu, P.-C., Centurioni, L., Shao, H.-J., Zheng, Q., Lu, C.-Y., Hsu, T.-W., & Tseng, R.-S. (2021). Surface current variations and oceanic fronts in the southern East China Sea: Drifter experiments, coastal radar applications, and satellite observations. *Journal of Geophysical Research: Oceans*, *126*, e2021JC017373. https://doi.org/10.1029/2021JC017373

Received 18 MAR 2021
Accepted 24 SEP 2021

© 2021. American Geophysical Union. All Rights Reserved.

Surface Current Variations and Oceanic Fronts in the Southern East China Sea: Drifter Experiments, Coastal Radar Applications, and Satellite Observations

Po-Chun Hsu[1], Luca Centurioni[2], Huan-Jie Shao[3], Quanan Zheng[4], Ching-Yuan Lu[5], Tai-Wen Hsu[6], and Ruo-Shan Tseng[3]

[1]Center for Space and Remote Sensing Research, National Central University, Taoyuan, Taiwan, [2]Scripps Institution of Oceanography, University of California, San Diego, San Diego, CA, USA, [3]Department of Oceanography, National Sun Yat-sen University, Kaohsiung, Taiwan, [4]Department of Atmospheric and Oceanic Science, University of Maryland, College Park, MD, USA, [5]Department of Marine Environmental Informatics, National Taiwan Ocean University, Keelung, Taiwan, [6]Center of Excellence for Ocean Engineering, National Taiwan Ocean University, Keelung, Taiwan

Abstract Ocean currents in the southern East China Sea (ECS) are complex and have long lacked systematic observational data. Observations from coastal radars in northern Taiwan, along with several drifters and satellite data, reveal a detailed ECS surface flow structure and thermal front. Drifter trajectories followed the seasonal flow field and were oscillatory and trapped due to strong tidal currents. Three drifters crossed the oceanic front off the northern coast of Taiwan following the tidal motion with a rapid change in the sea surface temperature by 2.5°C, which was recorded within a small distance of 500 m. A significant seasonal water mass exchange cycle occurred in the southern ECS. Starting in October, the Kuroshio Current intrudes onto the ECS shelf, causing the formation of a southwestward Northern Taiwan Coastal Current that mixes with the China Coastal Current to form a southward flow in the northern Taiwan Strait. Beginning in March, the ocean current off northwestern Taiwan shifts northward and then gradually flows eastward into the Kuroshio region. With satellite-derived and model-simulated surface currents contradicting each other over long periods of time, hourly coastal radar data have not only successfully explained the spatiotemporal variations in the sea surface temperature, salinity, and chlorophyll concentration observed by satellites but have also resolved the long-standing disputes over the surface currents in the southern ECS.

Plain Language Summary In the southern East China Sea (ECS), the ocean surface currents observed by satellite altimeters and estimated based on numerical models have considerably differed for a long time, especially in winter. The data observed by shore-based high-frequency radar have yielded new discoveries. Beginning in October, the Kuroshio Current intrudes onto the ECS shelf and pushes Kuroshio waters with high temperatures, high salinities, and low chlorophyll concentrations to the west, causing the current from northern Taiwan to flow southwestward into the Taiwan Strait (TS). Then, starting in March, ocean currents off northwestern Taiwan turn northward, and the water off northern Taiwan is pushed eastward back to the Kuroshio region. These flow field variations cause a significant oceanic front in the 121°E–122°E area in the southern ECS. We deployed four surface velocity program (SVP) drifters to observe the ocean flow and used virtual drifters to simulate the distribution probability of the track in each month. The drifters basically followed the movement direction of the seasonal flow field but could have been affected by the significant tidal currents and become trapped. With this study, we aim to better understand the southern ECS environment from a geophysical perspective.

1. Introduction

The East China Sea (ECS) is an area of importance in the Pacific-Asian Marginal Seas (Figure 1). The southern ECS plays an essential role in modulating ocean circulation and the exchange of water masses (Chen & Sheu, 2006; He et al., 2019; Hu et al., 2020), fishery resources (Naimullah et al., 2020), and biogeochemical materials (Chen, 2008; Liu et al., 2000; Yu et al., 2016) between the Taiwan Strait (TS) and Kuroshio Current (KC). The ECS shelf is in the northern waters of Taiwan and is a shallow platform with a width of 340 km and an average depth of 130 m. The long, narrow depression at the junction of the TS and southern ECS

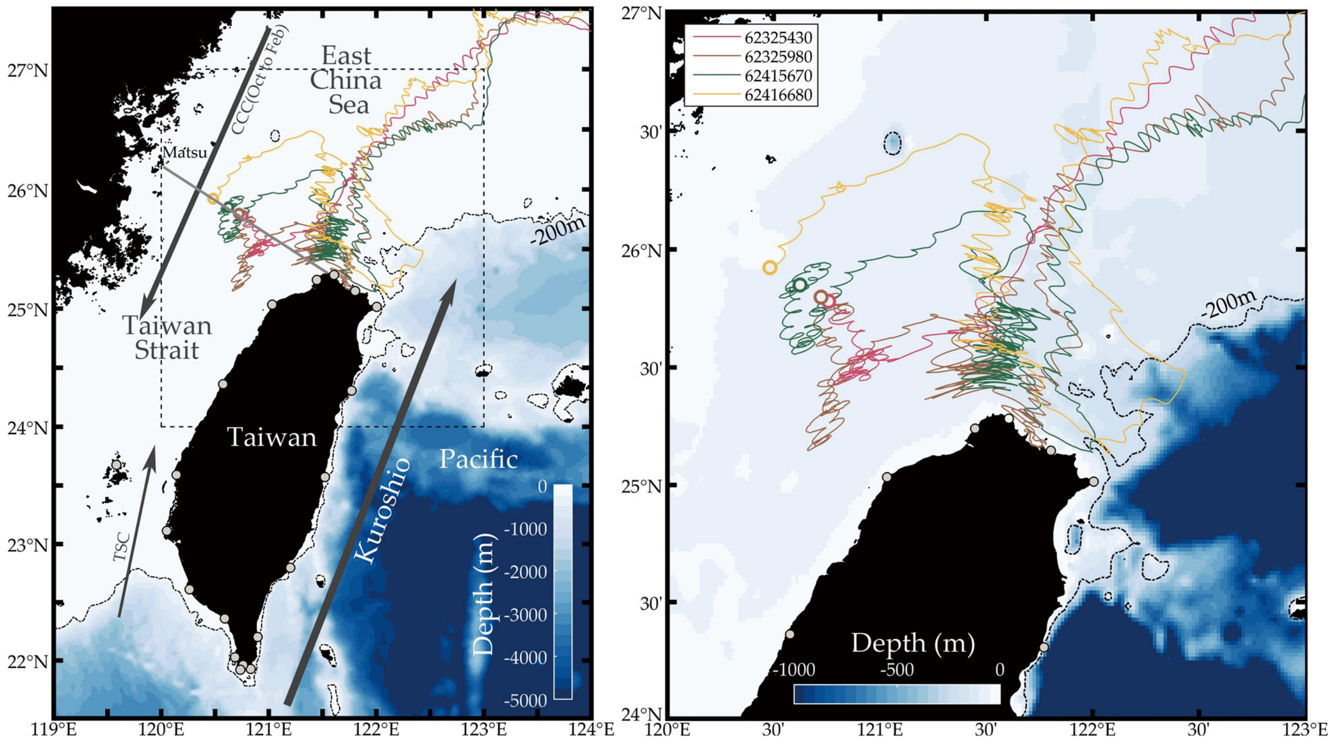

Figure 1. Study area with submarine topography obtained from the ETOPO1 1 arc-minute global relief model (doi:10.7289/V5C8276M). The colored circles and lines represent the deployed positions and trajectories of the drifter experiments, respectively. The gray dots represent the coastal radar station. The gray line between the northernmost tip of Taiwan and Matsu represents the virtual location of the junction between the southern ECS and the TS. The three arrows in the left panel show the main ocean currents: the China Coastal Current (CCC), the Taiwan Strait Current (TSC), and the Kuroshio Current (KC). Please note that the color scale in the left panel differs from that in the right panel to better highlight more detailed topography.

stretches from the northeast to the southwest and is approximately 300 km long with a water depth of more than 60 m. Regarding the characteristics of the water masses, the composition of the TS water is mainly affected by the Taiwan Strait Current (TSC) and the China Coastal Current (CCC) (Chang et al., 2006; Hu et al., 2010; Jan et al., 2010; Zhou et al., 2018). The surface current structure in the southern ECS can be influenced by tides; a semidiurnal tidal cycle occurs in the TS, and a mixed semidiurnal tidal cycle is seen off northern Taiwan (Lie & Cho, 2016). The tidal current flows westward during the flood phase and eastward during the ebb phase in the southern ECS (Jan, Chern, & Wang, 2002, Jan et al., 2004; Hsu et al., 2020).

Regarding the characteristics of the surface current field between the northern TS and southern ECS, Jan, Wang, Chern, and Chao (2002) suggested the presence of the southward CCC and the northward Kuroshio Branch Current (KBC) along the western and eastern boundaries of the TS, respectively, in the spring, the northward South China Sea monsoon current (SCSC) in the whole TS in the summer, and the southward CCC and northward SCSC along the western and eastern boundaries of the TS, respectively, in the fall. Hsu et al. (2018) further stated that part of the SCSC might flow along the northern coast of Taiwan and southeastward into the KC region in summer. However, there has been great divergence in the perceptions of surface currents in the winter. The CCC along the coast is mainly composed of low-temperature and low-salinity freshwater, whereas the upper KC is comprised of high-temperature and high-salinity water (Jan et al., 2010). Several studies have pointed out that the surface CCC could flow eastward toward northern Taiwan along the northeast side of the TS (Jan, Wang, Chern, & Chao, 2002, Jan et al., 2011; Wu et al., 2007). However, using nearly 30 years of historical satellite-tracked surface drifter data, Qiu et al. (2011) suggested that almost all winter drifters that enter the TS eventually move southward; i.e., the KC intrudes onto the ECS shelf (Hsin et al., 2011; Liu et al., 2014, 2020; Oey et al., 2010; Zhuang et al., 2020) and flows southward into the TS. The surface flow field results obtained from numerical modeling have also supported the southward flow of the northern TS in winter (Lin et al., 2016; Yu et al., 2016). Regarding more recent discoveries about the flow field in the northern TS, wind-induced coastal-trapped waves could affect circulation in the TS and intensify the southward intrusion of cold waters into the southern TS (Ko et al., 2003; Liao et al., 2017). Moreover, Zhang et al. (2020) found that the CCC became stronger in the winters after 1998, which could be attributed to the intensification of northeasterly winds, the weakening of TS warm water, and other oceanic-atmospheric interactions. Thus far, the status and characteristics of the winter ocean surface current field at the junction of the southern ECS and the TS have remained unclear.

Satellite altimetry, ocean current reanalysis, and numerical model output data have all shown that the surface structure of the flow field in the southern ECS is complex, with significant seasonal changes. Because of the low spatial and temporal resolutions of the datasets, it is difficult to determine the tidal variations and characteristics of ocean currents in the southern ECS, especially along the coast. However, since the northern waters of Taiwan are located at the intersection of the TS, ECS, and KC, with multiscale oceanic phenomena and fishery resources, it is necessary to clarify the dynamic characteristics of the ocean current field. The following questions arise. First, what are the monthly and seasonal surface flow field characteristics at the junction of the southern ECS and the TS, especially in the winter? Second, because ocean currents comprised of different water masses meet here, significant oceanic fronts are expected. Where and when do these sea surface temperatures (SSTs), sea surface salinities (SSSs), and chlorophyll fronts appear? Third, to better understand the mechanisms of oceanic phenomena in this area on a relatively small scale (Figure 1), is it possible to obtain detailed information about ocean currents with higher temporal and spatial resolutions?

To answer these questions, we use surface current field data derived from a coastal ocean dynamics application radar (CODAR) observation system (Roarty et al., 2019; Shen et al., 2019), incorporating surface velocity program (SVP) drifter data with a very high sampling interval. Satellite SST, SSS, and chlorophyll concentration data are also employed to investigate the oceanic fronts and how they are influenced by ocean currents. This study presents the results of our multi-time-scale observations of ocean currents and the frontal characteristics in the southern ECS. The results clarify the previously mentioned long-standing problems and inferences in this important marginal sea area and improve the understanding of the temporal and spatial structures of surface currents and oceanic fronts in the southern ECS. Data from various sources used in this study, particularly the CODAR system of Taiwan and our SVP drifter experiments, are described in Section 2. A comparison of ocean current fields derived from various sources in the southern ECS is presented in Section 3. Section 4 presents the results of SVP drifter experiments and a virtual drifter experiment based on CODAR data. Oceanic fronts are described in Section 5, followed by a discussion and concluding remarks.

2. Data and Methods

2.1. Ocean Current Field

Four ocean current observation products (satellite altimetry, reanalysis, historical cruise observation, and CODAR data) and numerical model output data were used in this study. The global ocean satellite altimeter gridded level-4 sea surface heights and derived surface geostrophic eastward and northward sea water velocity data with a 1/4° grid and a daily temporal resolution were provided by the Copernicus Marine Environment Monitoring Service (CMEMS). OSCAR (ocean surface current analysis real-time) data with a 1/3° grid and a 5-day temporal resolution were generated by Earth Space Research. The numerical model yields current field data obtained from the HYbrid Coordinate Ocean Model (HYCOM) + Navy Coupled Ocean Data Assimilation (NCODA) global analysis simulation results with a 1/12° grid and a daily temporal resolution. To compare and discuss the ocean current fields, these three datasets were first processed as monthly averages. The data used in this study cover the period from January 1993 to September 2019. The Ocean Data Bank (ODB) database has compiled various oceanographic data in the seas surrounding Taiwan (117°–125°E, 18°–27°N) since 1991, including data collected by R/V Ocean Researchers I, II, and III. The available acoustic Doppler current profiler (ADCP) data were then distinguished by the depths associated with each standard level number based on the World Ocean Database 2013 and transformed into a 1/4° grid in latitude and longitude. The Taiwan Ocean Radar Observation System (TOROS) was built along the coast of Taiwan by the Taiwan Ocean Research Institute, National Applied Research Laboratories (Roarty et al., 2019). The ocean surface currents were measured by 19 CODAR stations (including 13 operational sets of 5 MHz, 5 sets of 13 MHz, and one set of 24 MHz compact type high-frequency ocean radar instruments) around Taiwan more than 100 km from the coast with a 10-km spatial resolution and a 1-hr temporal resolution (Shen et al., 2019). The observation range of CODAR data covers the area between 119°E and 123°E and between 21°N and 26.5°N. The radial velocities from different radar sites were searched with a 15-km search radius at each grid point and combined with a compact, noncontact surface current and wave measurement of the CODAR SeaSonde high-frequency radar system to produce hourly surface current data. Based on the difference between the observed wave and the theoretical phase velocities of deep-water waves, the velocity and direction of the surface ocean current were calculated. The hourly data refer to the calculation of the observed radial velocity approximately 75 min before and after the moment of measurement. TOROS system maintenance work was performed at least once per year for antenna pattern measurements based on a multiple-signal classification algorithm (Lipa et al., 2006), and quality control of the optimized parameter data was conducted based on Barrick's et al. (1977) theory, including spatial and temporal uncertainty, the maximum, minimum and average velocities; and the spatial and temporal counts. The CODAR data were used to explain the ocean phenomena of the current fields north of Taiwan. The time span of the data used in this study was December 2014 to May 2020.

2.2. SVP Drifter Experiments

Eight SVP drifters with drogues at a nominal depth of 15 m were deployed in the middle of the northern TS by the ferry *Taima Star* on February 3 and 15, 2017 (Figure 1). Among them, four drifters were either picked up by fishermen or malfunctioned; only four drifters operated successfully, and their data were analyzed and reported in this article. The sampling interval was set to 15 min from the beginning of the study period to 25 March for close examination of oceanic features near Taiwan and then reset to 3 hr afterward to save battery power. A thermistor was mounted in the bottom part of each surface buoy. The bench accuracy of the SST measurements was ±0.05°C after a 5-point calibration was conducted across the sensing range of the thermistor (Centurioni, 2018). All of the drifters carried a satellite modem for data (SST and position) telemetry, which received the measured positions with a global positioning system engine. The current velocity was determined from the traveling distance divided by the time elapsed based on the centered difference method. The SVP drifters were designed and produced by the Lagrangian Drifter Laboratory at the Scripps Institution of Oceanography, and the observed data eventually joined the Global Drifter Program, which is part of the global ocean observation system maintained by the National Oceanic and Atmospheric Administration's Atlantic Oceanographic & Meteorological Laboratory. The start times (UTCs) of the four drifter observations were 18:44 on February 3, 2017 (Drifter-1; ID: 62325430), 18:53 on February 3, 2017 (Drifter-2; ID: 62325980), 19:04 on February 3, 2017 (Drifter-3; ID: 62415670), and 20:02 on February 15, 2017 (Drifter-4; ID: 62416680).

2.3. Temperature, Salinity, Chlorophyll Concentration, and Wind Field

The Group for High-Resolution Sea Surface Temperature (GHRSST) multiscale ultrahigh-resolution level-4 global foundation SST analysis data (version 4.1), which were generated by combining complementary satellite and in situ observations within optimal interpolation systems with high spatial resolutions, were used to analyze the SST fronts. The GHRSST level-4 global 0.01° grid data were produced by the National Aeronautics and Space Administration's Jet Propulsion Laboratory from several instruments, such as advanced microwave scanning radiometers, moderate-resolution imaging spectroradiometers, WindSat radiometers, and in situ SST observations. The Soil Moisture Active Passive (SMAP) Sea Surface Salinity, version 4.0, validated data observed from the L-band radiometer with a 1/4° grid, and a monthly temporal resolution was used to analyze SSS fronts. The near-polar orbit of SMAP allows the instrument to obtain complete global coverage of the oceans in three days, with a repeat cycle of eight days. The Geostationary Ocean Color Imager (GOCI) chlorophyll concentration data had a spatial resolution of approximately 500 m over the northeast Asian marginal sea. The observation time in the southern ECS was 0:00 to 7:00 (UTC), and the local time was 8:00 to 15:00 (UTC+8). The level-2 hourly chlorophyll concentrations in seawater, assessed by ocean color index algorithm data products, were used to analyze the ocean chlorophyll fronts. The Advanced Scatterometer (ASCAT) data (version 2.1) were produced by remote sensing systems and are funded by the NASA Ocean Vector Winds Science Team. Daily and time-averaged (3-day, weekly, and monthly)

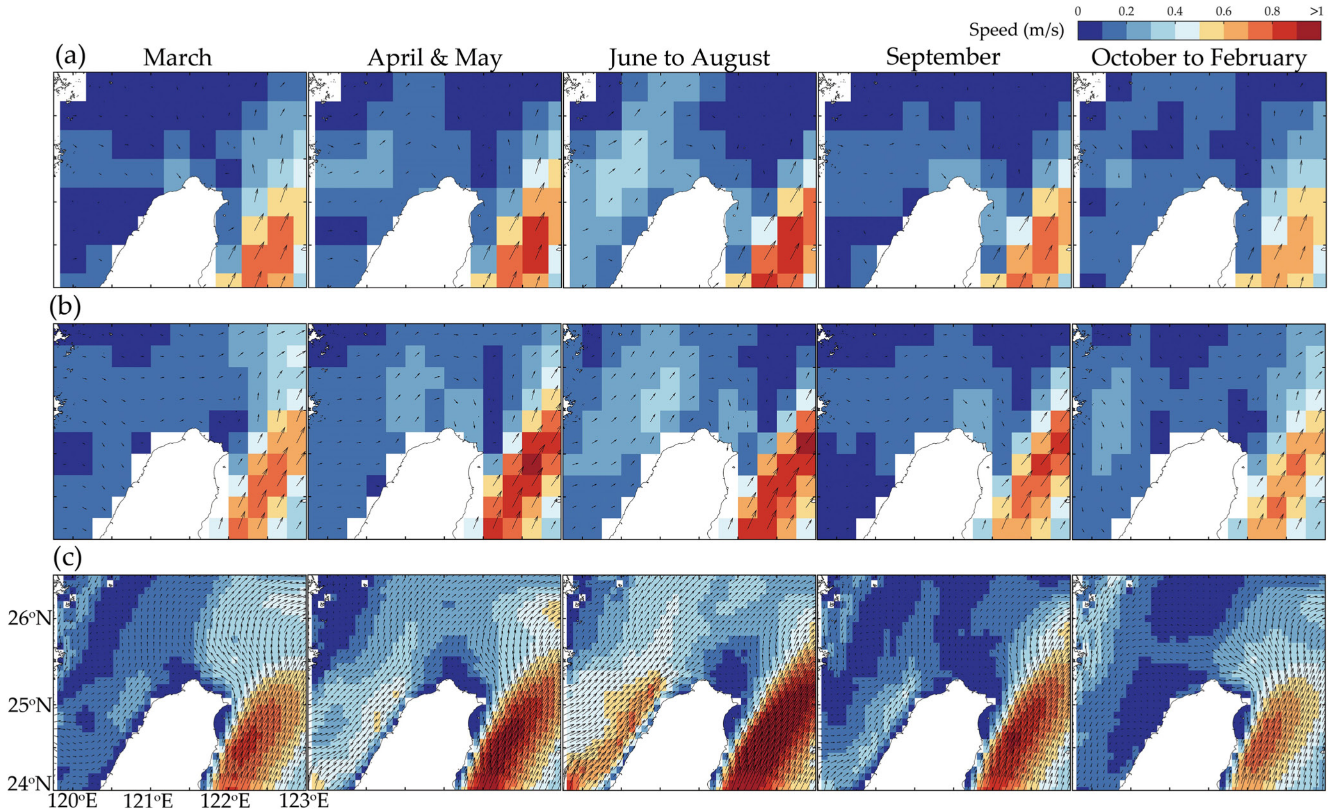

Figure 2. Climatological seasonal ocean surface flow fields obtained from various databases: (a) OSCAR, (b) CMEMS, and (c) HYCOM. The climatological seasonal ocean surface flows are averaged over the period of January 1993 to September 2019.

0.25° gridded data containing wind speeds and directions 10 m above the water surface were used to analyze the surface wind field.

2.4. Ocean Current Adjacent to the Southern ECS

Three commonly used ocean current databases-OSCAR, CMEMS, and HYCOM-were employed in this study to observe the ocean surface current variations in the southern ECS. According to the characteristics of the ocean currents (Figure 2) and ocean surface wind field (Figure 3) in northern Taiwan, the months could be divided into three periods: April–May, June–August, and October–February. March and September are the transitional months. The prevailing wind in this region from October to February is the strong

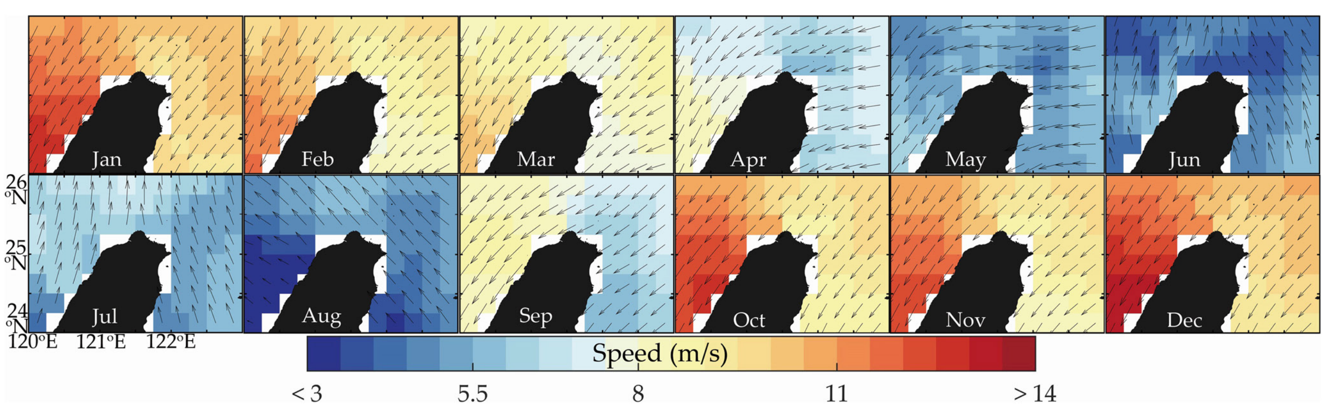

Figure 3. Climatological monthly wind fields averaged over the period of March 2007 to October 2020.

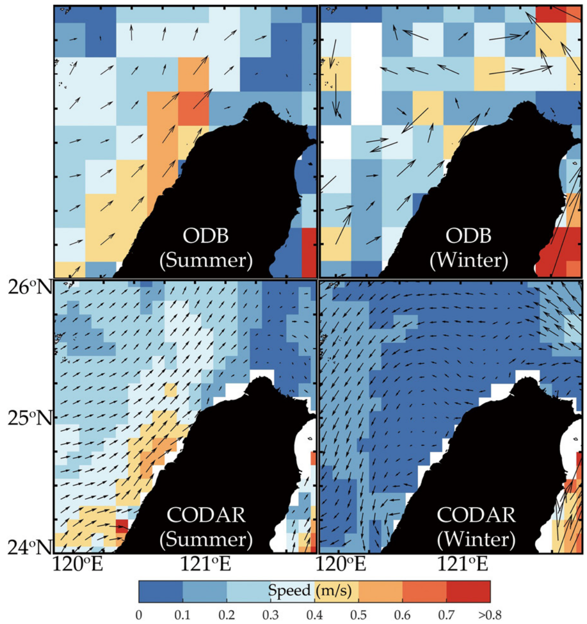

Figure 4. Climatological near-surface ocean current of ODB and surface current of CODAR in winter and summer. Please note that the difference in vector sizes only represents the direction.

northeasterly monsoon with a wind speed of 8–12 m/s. Southwesterly monsoons prevail in summer from June to August with wind speeds of 3–6 m/s from the south or southeast. April and May are the transitional months from the winter monsoon to the summer monsoon with wind speeds of 4–8 m/s coming from the northeast or east. Figure 2 presents the climatological monthly average flow fields in the southern ECS obtained from the different databases from January 1993 to September 2019. The KC flowed northward throughout the year off eastern Taiwan, as consistently observed in all three databases. The main axis of the KC had a fast velocity from June to August (0.87–1.09 m/s) and a slow velocity from October to February (0.67–0.78 m/s). However, inconsistent flow field patterns were found in other locations in this region. These patterns significantly affected our understanding of the source of the water in the southern ECS, especially since this area represents the confluence of the TS, ECS, and KC waters. The inconsistent features observed mainly included three conditions. (a) From March to May, the strong KC that intruded onto the ECS shelf was only observed in the HYCOM simulation. Moreover, the OSCAR and CMEMS data revealed that the flow field was mainly oriented southeastward along the coast, whereas the HYCOM simulation showed a northwestward flow along the coast off northeastern Taiwan. (b) From June to September, the current in the TS flowed toward the KC region along the northern coast of Taiwan, which was observed in both the OSCAR and the CMEMS data but not in the HYCOM simulation. (c) From October to February, only the CMEMS data showed that the ocean currents in the southern ECS mainly flowed eastward from the TS to the KC, whereas the HYCOM simulation showed that the ocean currents in this region mainly flowed westward from the KC to the TS.

Significant differences in ocean surface currents can be observed for the southern ECS between the satellite-derived data and HYCOM simulation. In the winter and spring, research surveys have difficulty continuously measuring ocean currents due to poor sea states. Although the ODB has accumulated nearly 30 years of data, there are still insufficient data in the southern ECS. The surface current field derived from the CODAR system of TOROS was used in this study to clarify the flow field characteristics. The CODAR data accumulated over the past 5 years have provided continuous and detailed flow information in the southern ECS, and the data can be very useful for examining the ocean current dynamics on various time scales, including hourly, daily, and monthly scales, which were not previously possible. Figure 4 presents the near-surface ocean currents obtained from ocean research surveys from 1991 to 2020 and surface ocean currents observed by CODAR from December 2014 to May 2020. In the summer, the flow directions and velocities of the two datasets are similar, but the ocean current observed by ODB is two times faster than that observed by CODAR, especially off northwestern Taiwan. In the winter, due to the lack of observational data, the ODB ocean current field data are not suitable for further discussion.

The seasonal CODAR surface flow maps in the southern ECS are presented in Figure 5. From March to September, two branches of the TSC existed in northwestern Taiwan (121°E, 25.5°N). One branch flowed northward into the ECS. Its speed was faster from June to August, reaching a mean value of 0.5 m/s, whereas in March the speed was only 0.2 m/s. The other branch flowed slowly at 0.1 m/s eastward along the northern coast of Taiwan toward the KC northeast of Taiwan. From October to February, the KC intruded onto the ECS shelf, and some portion of the intrusion flowed westward along the northern Taiwan coast into the TS. During this period, the ocean surface currents in the TS flowed toward the south. The location of the significant KC intrusion was slightly north of 25.5°N, with a speed of 0.4 m/s. The flow velocity in the central part of this figure, i.e., from the southern ECS to the northern coast of Taiwan, was slow, averaging <0.1 m/s. In March, the KC continued to intrude onto the ECS shelf; however, the ocean surface currents in the TS converted to flowing northward, and the coastal waters of northern Taiwan also turned eastward from the TS to the KC.

10.1029/2021JC017373

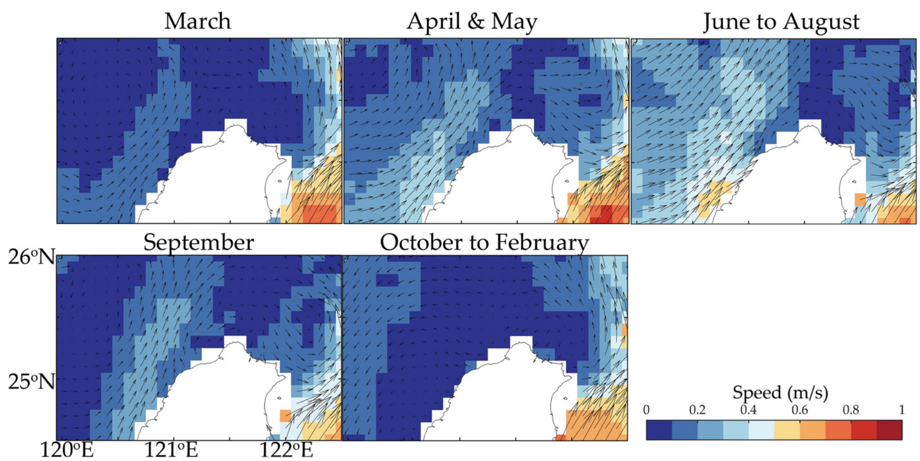

Figure 5. Climatological seasonal surface flow fields of CODAR averaged over the period of December 2014 to May 2020.

A simple image representation can be used to understand the characteristics and sources of the current variations in both the TS and KC. Figure 6 shows the probability distribution of the westward flow (east-west component <0) calculated using the hourly CODAR data. The grid data are displayed only when the missing data of the grid point are <30% over the entire period. As expected, the flow field in the southern ECS was characterized by seasonal ocean currents and tidal currents, and the KC flowed northward off eastern Taiwan throughout the year. Combining the CODAR monthly flow field results with the results of previous studies (Hsu et al., 2018; Jan, Wang, Chern, & Chao, 2002; Oey et al., 2010; Qiu et al., 2011), we have provided a diagram of the dynamic mechanism of the main ocean surface currents in the southern ECS (Figure 6). The semidiurnal tidal current in the southern ECS was characterized by westward flow during flood tides and eastward flow during ebb tides (Hsu et al., 2020). The probabilities of eastward and westward tidal currents off northern Taiwan were approximately 50%, and it was expected that currents from the TS and KC sides would be affected by significant tidal currents and that drifters would become trapped in this area when flowing through the region north of Taiwan. In the area between the KC and the northern coast of Taiwan, the Northeastern Taiwan Coastal Countercurrent (NETCC) existed throughout the year and flowed from the ECS shelf along the coast to the KC region (Hsu et al., 2018; Yin et al., 2020).

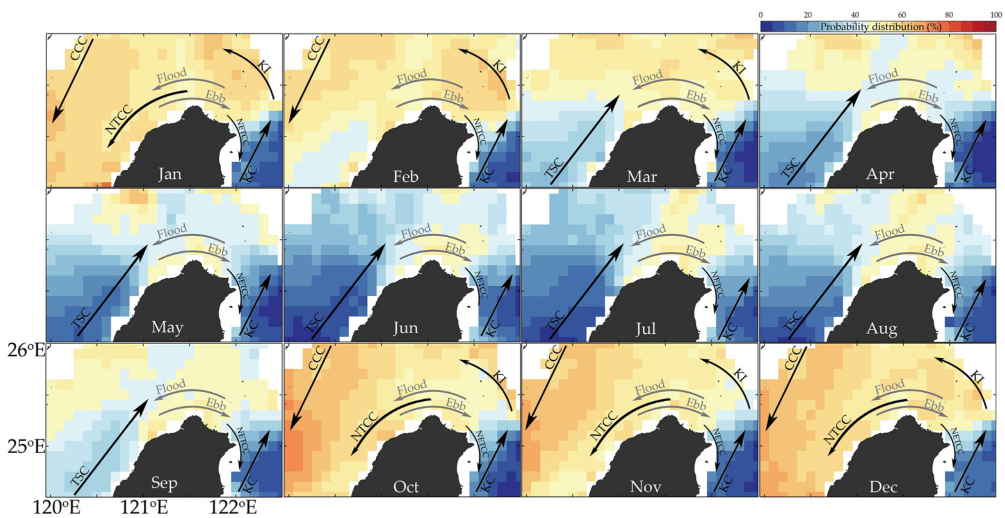

Figure 6. Schematic diagrams of the ocean surface current characteristics in the southern ECS. The background color is the probability distribution (%) of the westward flow, calculated from hourly CODAR data from December 2014 to May 2020.

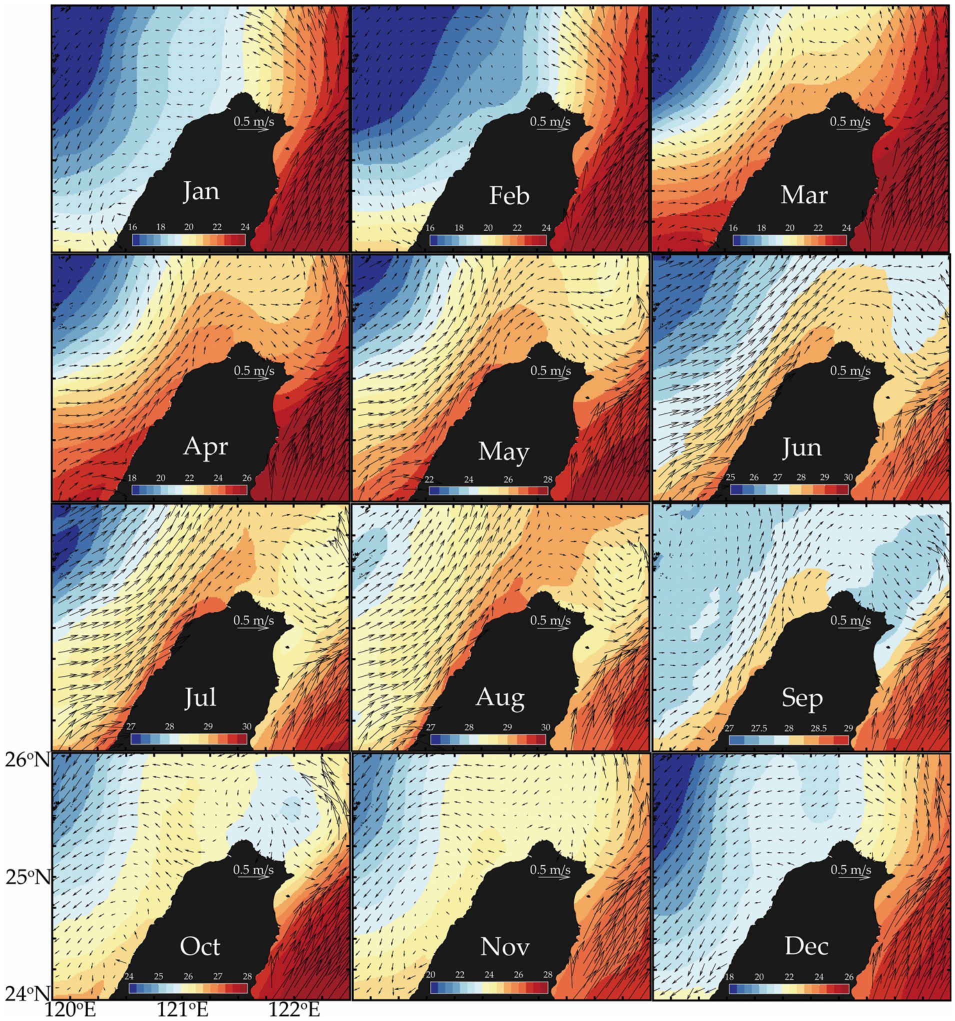

Figure 7. Monthly SSTs (°C) and the CODAR flow field from December 2014 to May 2020.

In the northern TS, the main current from April to August is the TSC. The characteristics of these water masses could be different in months, but all displayed flow directions from south to north. The characteristics of the flow field at the intersection between the southern ECS (the northern waters of Taiwan) and the TS diverged in winter when comparing the results of the ocean current databases (Figure 2) with those of previous studies (Jan et al., 2011; Qiu et al., 2011). Jan et al. (2011) suggested that the primary source of ocean currents at the junction between the northern waters of Taiwan and the TS is the eastward winter monsoon-driven CCC, similar to altimeter-derived ocean surface currents (Figure 2). However, based on historical drifter data, Qiu et al. (2011) suggested that the currents in this area are mainly caused by the KC spilling onto the ECS shelf and flowing westward along the northern coast of Taiwan into the TS, consistent with the HYCOM simulation (Figure 2). In this study, the results of the continuous hourly observations of ocean currents based on CODAR suggested that, during the winter, the currents between northern Taiwan and the TS are mainly caused by the KC spilling onto the ECS shelf and passing through the tidal current area before flowing southwestward into the TS. We named this westward surface current the Northern Taiwan Coastal Current (NTCC), and this current had an average velocity of 0.1–0.2 m/s.

We further combined the CODAR surface flow with the SST images obtained during the same period (Figure 7) to further analyze the influence of the monthly average ocean current on the characteristics of SST changes in the southern ECS. We started by examining the flow field and the SST cycle from September, when the flow field during the seasonal transition period has no significant characteristics. The northward current in the TS began to weaken, and a southward CCC began to appear adjacent to the coast of China in the southern ECS. The SST at the southern end of the ECS was less than 28°C, and the oceanic front was almost nonexistent. From October to March, the KC intrusion (KI) spilled onto the ECS shelf, affecting the entire flow field in the southern ECS. KI refers to the northward or northwestward ocean current extending from the KC into the ECS. In October, the flow direction on the TS side began to turn to the south. These flows were mainly composed of the CCC along the coast of China and the NTCC along the coast of Taiwan and had a velocity of approximately 0.2 m/s. The SST of the CCC was 2–4°C lower than that of the NTCC, especially from November to January. Upon combining the ocean current and SST observations, it is evident that the KI flowed westward at the southern ECS, promoting a warm KC, mixing with cold water from the north and forming a significant SST front in the north-south direction. At 200 km of equal latitude, the SST varied by >8°C. In February, the NTCC began to weaken and disappear. In March, the northward current in the TS entered from the Luzon Strait through the southwest coast of Taiwan, bringing warm seawater before it, and it lasted until September. The counterclockwise flow field observed off the northeastern corner of Taiwan is a common phenomenon called a cold dome, which is a year-round phenomenon in the subsurface but is exposed to the sea surface from June to October (Cheng et al., 2009; Wu et al., 2008). The SST in the southern ECS can reach 28°C–29°C, and the oceanic front in summer generally appears close to the coast of northern Taiwan (between 121.5°E and 122°E).

2.5. SVP Drifter Experiments in the Southern ECS

2.5.1. Drifter Trajectory

To further understand the dynamic process of ocean currents in the southern ECS, four SVP drifters were deployed in February 2017 at the junction of the TS and southern ECS to monitor the flows and SST of this region. Drifter-1, Drifter-2, and Drifter-3 were deployed on 4 February in sequence at 2:33, 2:40 and 3:04 local time (UTC+8), respectively, from a sailing ferry in the northern TS. The distances of starting positions between Drifter-1 and Drifter-2 and between Drifter-2 and Drifter-3 were approximately 3.9 and 11.4 km, respectively. Drifter-4 was deployed on 16 February. The trajectories and weekly positions of these four drifters for the first three months after deployment are illustrated in Figure 8. The drifter velocities and the observed SST are illustrated in Figures 9 and 10, respectively. Drifter-2 and Drifter-3 had somewhat similar trajectories, and their separations remained between 13 and 66 km. Both drifters first moved slowly and lingered toward the south for the first week, responding to the intensified northeasterly monsoon, and then they moved toward the east to the northern Taiwan waters, where they oscillated back and forth in the E-W direction carried by the strong semidiurnal tidal currents and were "trapped" just off the cape for approximately three weeks. Finally, the drifters broke free from the tidal currents. These two drifters traveled to the coastal water northeast of Taiwan, where pronounced SST increases were observed (Figure 10b and 10c). Then they moved in a cyclonic fashion toward the north, where the waters were much warmer, and the flows were tide dominated (Figures 9b and 9c). Subsequently, these drifters apparently merged into the northeast-bound Kuroshio Mainstream. The counterclockwise circulation northeast of Taiwan was also reported in earlier studies (Tang et al., 1999; Tseng & Shen, 2003).

Drifter-4 was deployed 12 days later 11.8 km northwest from Drifter-3's released position. Drifter-4's trajectories were similar to those of Drifters-2 and -3, except without lingering in the TS for the first week and without being trapped in the significant tidal area just off the cape for an extended period of time. The interaction with a sharp SST front, cyclonic circulation northeast of Taiwan, and warm and tidally dominated waters were also experienced by Drifter-4.

Although Drifter-1 was deployed only seven minutes earlier than and at a short distance (3.9 km) east of Drifter-2, the trajectories of these two drifters differed significantly, and the separations increased considerably with time, exceeding 600 km after 10 weeks. Drifter-1 first moved eastward for one week and then deflected toward the north to the southern ECS, where flows tidally dominated. Note that this area of significant semidiurnal tides was visited by all four drifters but at different times: late February for Drifter-1, early April for Drifter-2 and Drifter-3, and mid-March for Drifter-4. Nevertheless, the SST values in this area observed by these four drifters were quite different (Figure 10), that is, colder (~17°C) for Drifter-1 and warmer (>20°C) for the other three drifters. In other words, Drifter-1 remained in the cold-water masses, while the other three drifters crossed the SST front from the cold coastal waters to the warm KC waters. In summary, the trajectories of these four drifters and the observed SST revealed several interesting features,

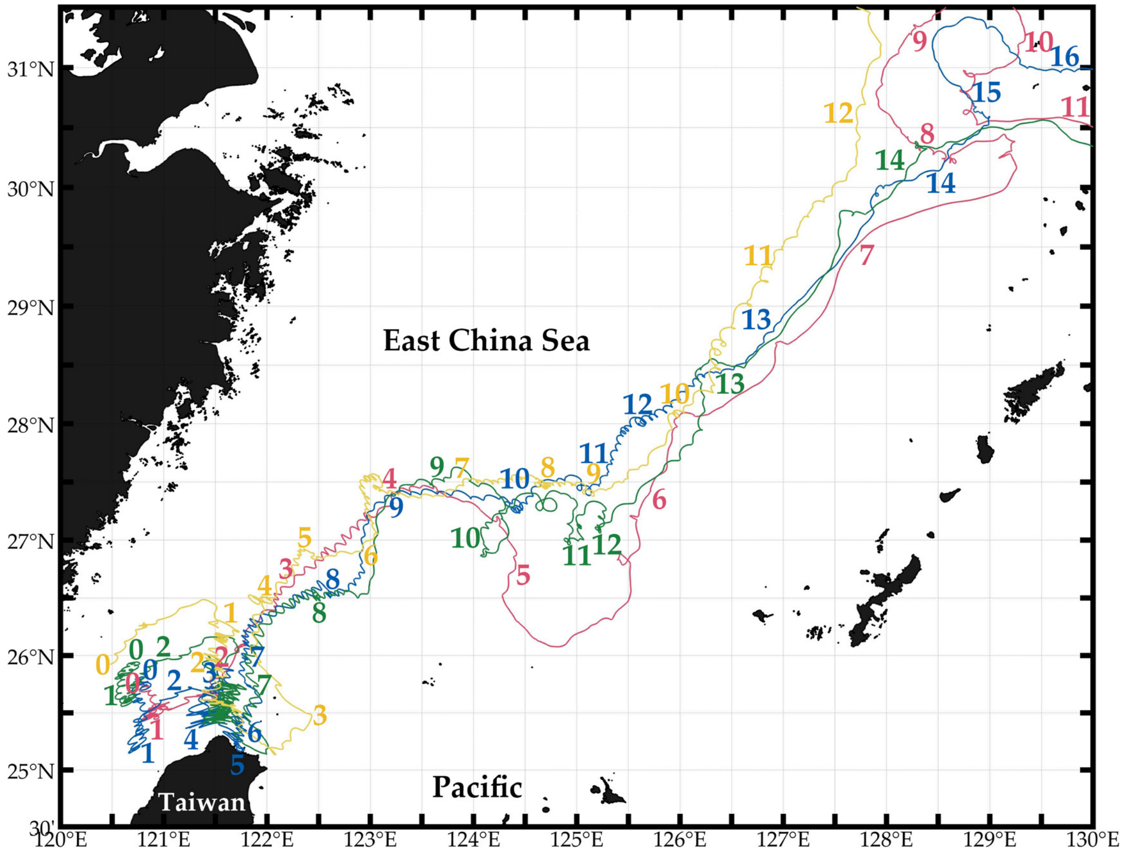

Figure 8. The weekly positions of the four drifters after deployment: Drifter-1 (red), Drifter-2 (blue), Drifter-3 (green), and Drifter-4 (yellow). The numbers represent the number of weeks since each drifter was deployed. For Drifter-3, the second to sixth weeks are not shown, when it was located off northern Taiwan.

such as the interaction of CCC, TS outflow, and KI in the southern ECS, as well as intense tidal currents and the existence of a pronounced SST front in the winter. The complicated flow patterns in this area resulted in diversified drifter trajectories, although their deployment positions and times were similar. Detailed flow velocities and observed SSTs of these four drifters are described in the next section.

2.6. Ocean Current Structure and SST Features Observed by SVP Drifters

The important phenomena observed from the four drifters in the southern ECS were selected for detailed analysis and discussion. First, we focused on the complicated results of the drifting trajectories of Drifter-2, Drifter-3, and Drifter-4. Drifter-2 (ID: 62325980) flowed southward at an average velocity of 0.44 m/s for a week and then turned back northward at 0.50 m/s after it was deployed at the northern TS (Figure 9b); it lingered in the TS for 13 days before heading east into the southern ECS (Figures 11a–11d). A northeasterly wind with a speed of 10.5 m/s was observed in this area. Although the SST in the region is affected by the tidal current north of the TS, the observed SST varied by only 1°C because the drifter SST remained in the same water mass region. The drifter was still affected by a significant tidal current after entering the southern ECS; this current flowed at 0.53 m/s adjacent to the 100-m isobath, reached the northernmost end of its path on 23 February, and then flowed southward at 0.87 m/s to the northern coast of Taiwan. There was a northeasterly ocean surface wind observed in northern Taiwan during the month of the study with an average speed of 8.4 m/s. Note that this drifter was stuck near the coast from 6 to 15 March, which could be seen from the sudden decrease in drifter speed to nearly zero (Figure 11h). Fortunately, this drifter broke free and subsequently resumed operating. From the two trapping processes experienced by the drifter in the TS and the southern ECS, we can conclude that the flow velocity was slow during one period and suddenly increased during the other period. This flow velocity transition was caused by neap and spring tides.

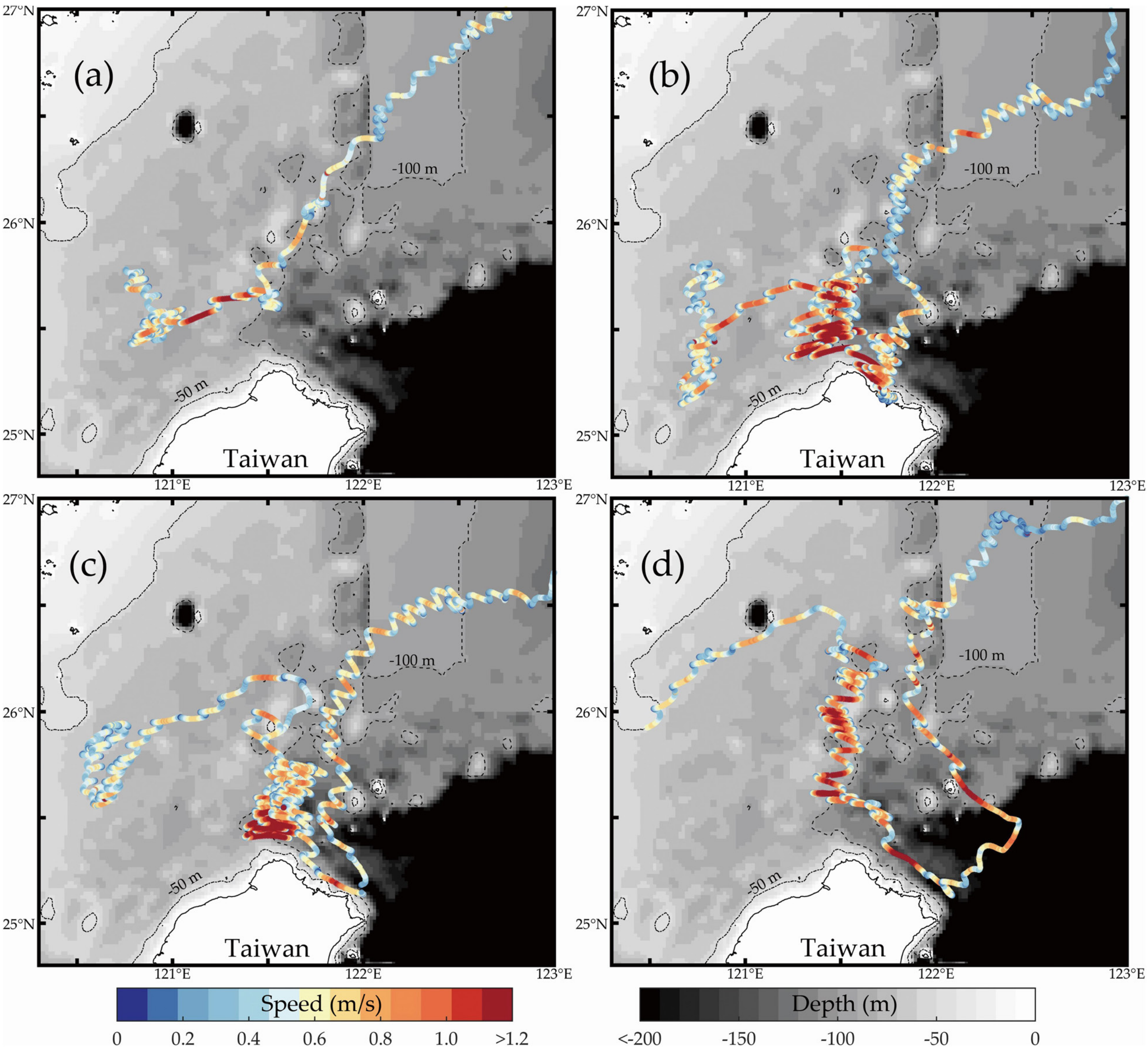

Figure 9. The observational flow speed along each drifter's trajectory: (a) Drifter-1, (b) Drifter-2, (c) Drifter-3, and (d) Drifter-4.

In areas with semidiurnal tides around Taiwan, the spring tide period is defined using the lunar calendar from the 29th to the 4th and from the 14th to the 19th of each month based on the long-term average tidal observations obtained in coastal areas by the Central Weather Bureau of Taiwan. During this study period, the spring tide period was from 10 to 15 February and from 25 February to 1 March. Different evolutions of flow velocity between two periods of 4–16 February and 17 February–23 March are shown in Figures 11d and 11h. In addition, two significant SST changes were observed when the drifter moved adjacent to the coast of northern Taiwan (Figures 11e and 11g). The first change occurred on 5 March, when the drifter flowed eastward with ebb currents and then westward with flood currents; significant SST variations were observed in this short time. While drifting eastward, the SST increased from 17.15°C to 19.66°C with only a 0.47-km drifting distance; then, the drifter flowed back westward, and the SST dropped to 17.13°C within 1.87 km. The second change was observed during the drifter departure from the coast from 14 to 15 March; the SST increased slowly from 16.97°C to 18°C. These abnormal SST changes were most likely caused by the drifter flowing back and forth across the oceanic front between the coastal water and the KC. The drifter gradually reached the KC after 15 March and continued to flow northward in the direction of the KC; the observed SST increased from 18°C to 21°C during this time. From this Drifter-2 experiment, it was found that

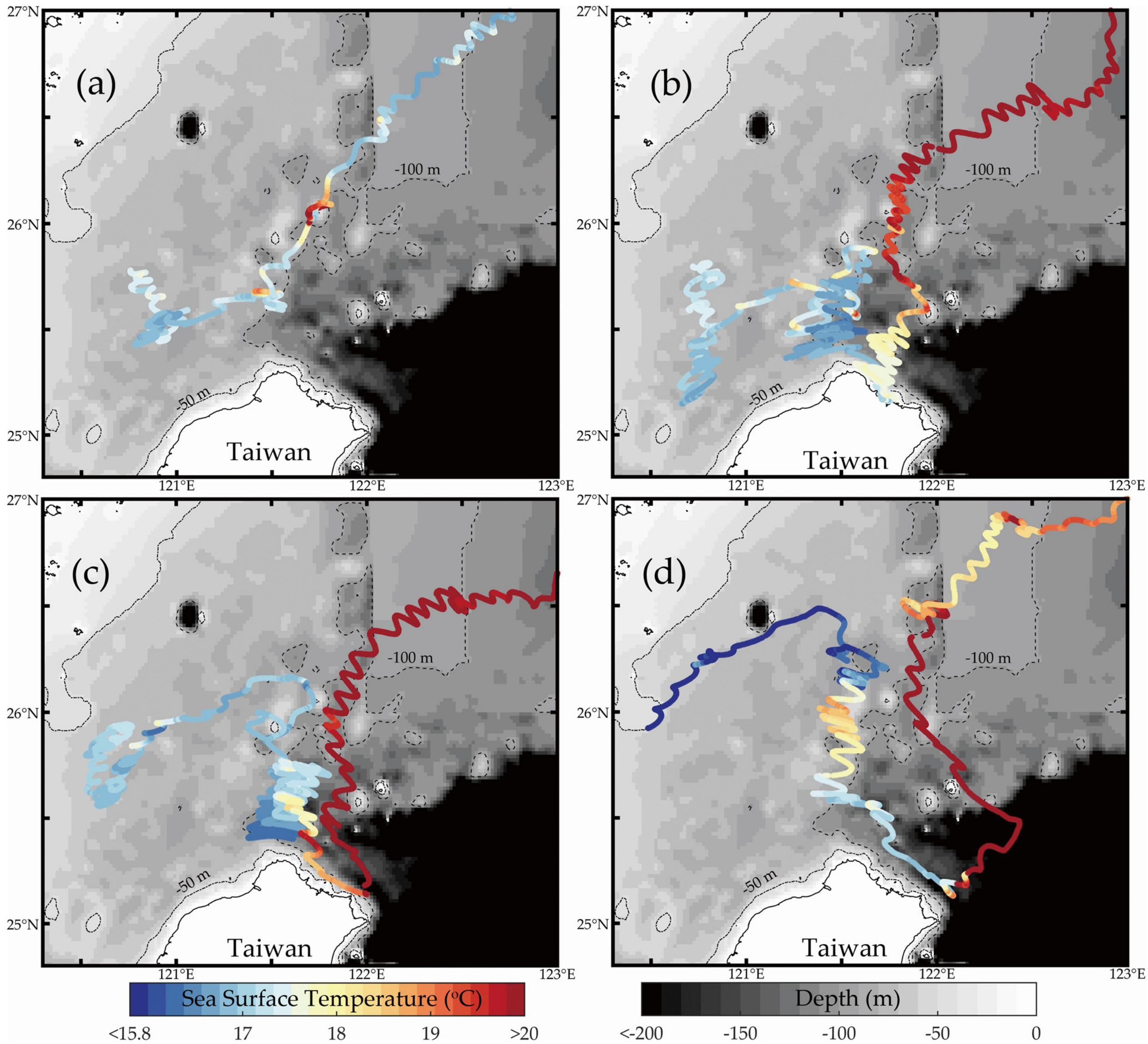

Figure 10. The observational SST along each drifter's trajectory: (a) Drifter-1, (b) Drifter-2, (c) Drifter-3, and (d) Drifter-4.

the drifter was trapped and rotated by the tidal current, and the observed change in its speed was related to the spring and neap tides (Figure 11f). A significant oceanic front formed at the intersection of different water masses in the southern ECS.

Drifter-3 (ID: 62415670) flowed southward in the TS with the tidal current and then returned to the north from 11 to 12 February (Figure 9c). A northeasterly wind with a speed of 10.4 m/s was recorded in this area. According to the OSCAR data, the direction of the ocean current was southward from 3 to 11 February and northward after 12 February, indicating that the drifter oscillated with the tidal current but was mainly affected by the direction of the flow field, causing it to drift northward and southward (Figures 12a–12d). The velocity of the drifter was affected by different tidal cycles: the drifter had a velocity of 0.46 m/s during the spring tide period and a velocity of 0.38 m/s at other times (Figure 12d). The drifter followed the ocean current and entered the southern ECS on 24 February, where it was trapped for 1 month by significant tidal currents (Figures 12e–12h). A northeasterly ocean surface wind was recorded in northern Taiwan during this month, with an average speed of 8.5 m/s. The drifter activities of the between 23 February and 19 March included two spring tide periods, and the average flow velocities were 0.88 m/s (25 February to 1 March) and 0.58 m/s (11 to 16 March) during these periods; the velocity was 0.53 m/s during the rest of the

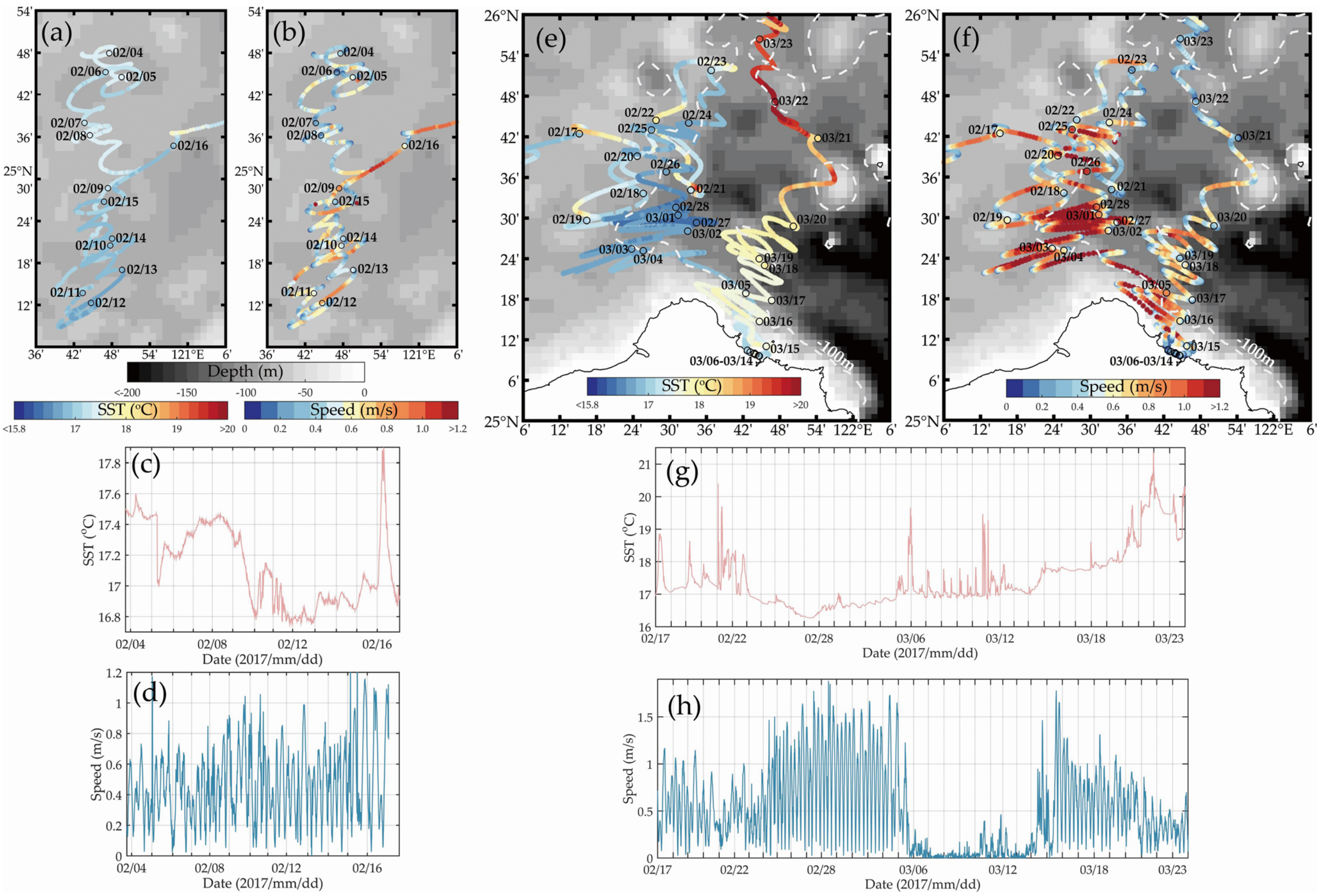

Figure 11. The observational SST and flow speed along Drifter-2's trajectory and corresponding time series plot: (a)–(d) in the TS from 4 to 16 February 2017 and (e)–(h) in the southern ECS from February 17 to March 23, 2017.

period (Figure 12h). The drifter broke free from the tidal current and drifted southeastward on 19 March, and then it flowed parallel to the northeastern coast of Taiwan into the KC. Afterward, it turned to drift northward toward the center of the ECS under the effect of the strong KC on 22 March (Figure 12g). During this period, the drifter observed two SST changes (Figures 12e and 12f). During the first change, the SST slowly increased from 17.9°C to 20.1°C within 8.2 km after the drifter broke away from the tidal current on 20 March. The second change was recorded when the drifter flowed southeastward into the KC and then turned northward off the northeastern corner of Taiwan, where the SST rose from 19.1°C to 22.7°C within 4.9 km. The two SST events were speculated to be due to the drifter flow across the oceanic front.

Drifter-4 (ID: 62416680) was deployed to the northwest of Drifter-2 and Drifter-3, and its release time was 12 days later than that of the previous two drifters. Based on the results of the first two drifters, it could be expected that Drifter-4 would also be affected by the tidal current. The drifter flowed northward at a speed of 0.47 m/s until 20 February and then turned southward and entered the waters of northern Taiwan (Figures 13a–13d). A northeasterly wind with a speed of 7.8 m/s was recorded in this area. The drifter observed interesting SST variations in this region. The SST rose from 15.9°C to 19°C and then dropped back to 16.9 C from 25 February to 3 March (Figure 13c). Based on the flow field and GHRSST data, the high SST recorded in this region was caused by the KC intruding onto the ECS shelf. The KI cut off the cold-water linkage between the southern ECS and the coast of Taiwan. Unlike Drifter-2 and Drifter-3, which were trapped by tidal currents for more than two weeks, Drifter-4 flowed in the northern waters of Taiwan for 13 days and then headed to the KC. A northeasterly wind with a speed of 9 m/s was observed in this area. The drifter flowed through the intersection of the coastal current and the KC and moved back and forth along the oceanic front (Figures 13e–13h). The SST was observed to rise from 16.9°C to 19.4°C within 0.8 km; the drifter then followed the tidal currents and returned to the cold-water region, with the SST slowly dropping back to

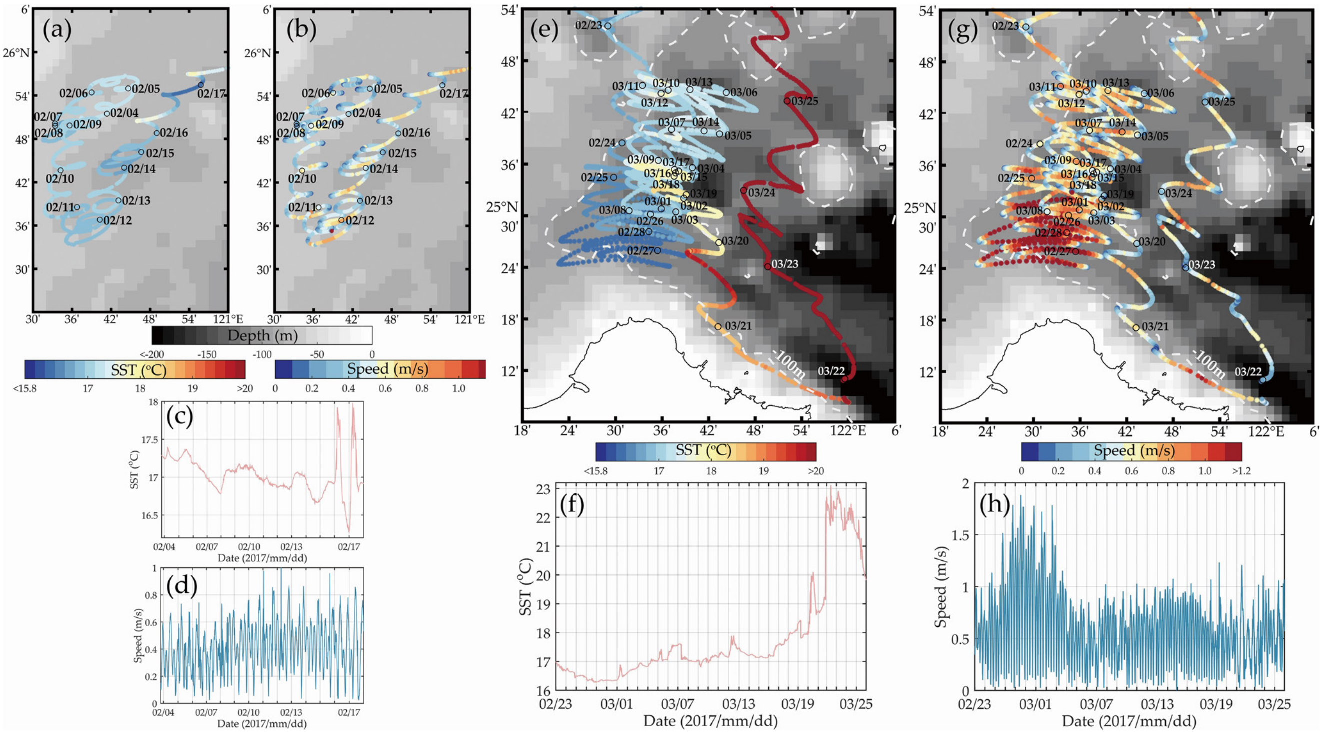

Figure 12. The observational SST and flow speed along Drifter-3's trajectory and corresponding time series plot: (a)–(d) in the TS from 4 to 17 February 2017 and (e)–(h) in the southern ECS from February 23 to March 25, 2017.

17.3°C. Then, the SST rose to 20.6°C within just 1.8 km as the drifter once again followed the tidal currents and returned to the cold-water region, where the SST dropped back to 18.2°C within 7.1 km. Subsequently, the SST rose again to 23.1°C within 1.2 km. Finally, the drifter moved northward along the KC with a stable SST (Figure 13g).

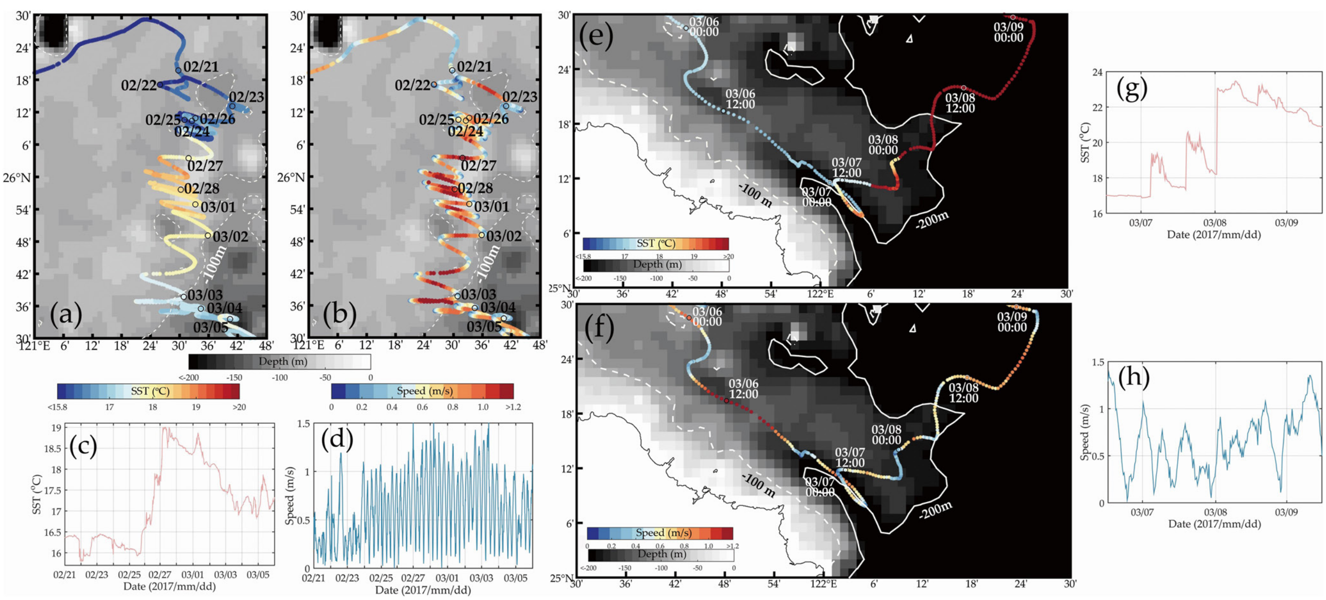

Figure 13. The observational SST and flow speed along Drifter-4's trajectory and corresponding time series plot: (a)–(d) in the southern ECS from February 21 to March 5, 2017 and (e)–(h) in northeastern Taiwan from 6 to 19 March 2017.

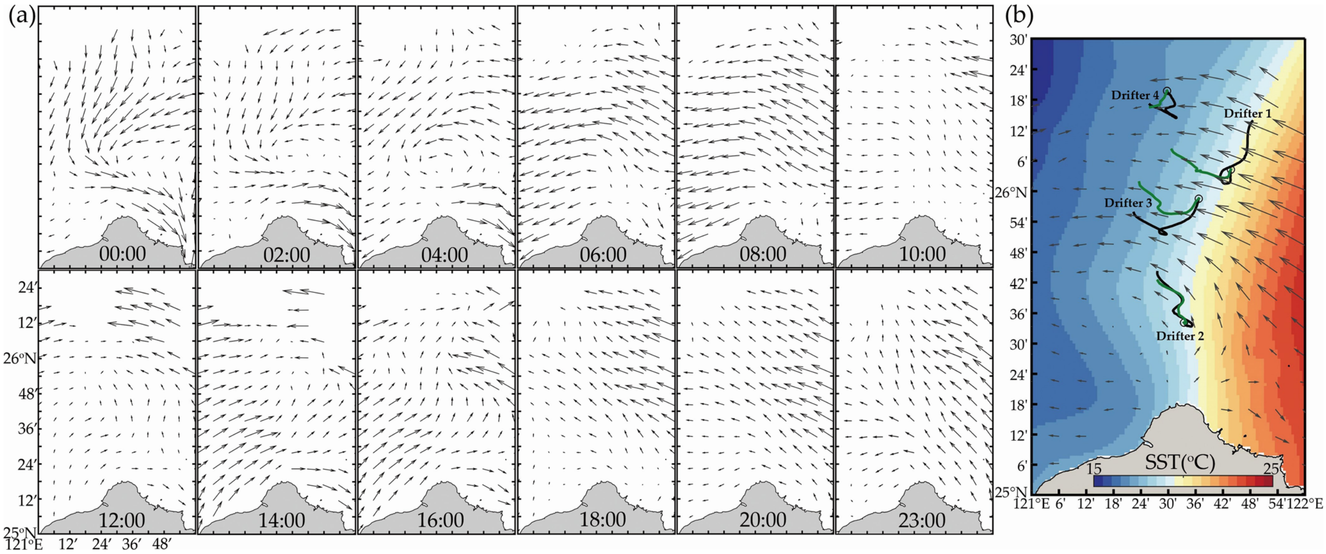

Figure 14. (a) The hourly CODAR surface flow in the southern ECS on February 21, 2017. (b) Trajectories of Drifters 1–4 (black lines) and corresponding virtual drifters (green lines) with daily CODAR surface flow (arrows) and GHRSST data (shading) on February 21, 2017.

The trajectory of Drifter-1 (ID: 62325430) was significantly different from those of the other three drifters. Drifter-1 flowed along the direction of the tidal current and flow field, was trapped in northwestern Taiwan for only 9 days, and then entered the southern ECS (Figures 9a and 10a). Unlike the other three drifters, which flowed southward after entering the southern ECS, Drifter-1 instead moved northward and drifted into the ECS at a speed of 0.46 m/s within a month after deployment.

The four drifters mainly flowed in the southern ECS from February to March, and the results could be summarized as a series of processes that correspond to the conceptual diagram of the flow field shown in Figure 6. The processes that occurred after the drifters were deployed in the TS could correspond to low-frequency ocean currents, such as the southward CCC, the northward TSC, coastal currents, and the connection of the northward KC. These low-frequency and stable ocean currents fluctuated due to high-frequency tidal currents, that is, flood and ebb tidal currents. According to drifter experiments, several important new discoveries could be made. There is a significant tidal current in the southern ECS, and its speed changes are related to the cycles of the spring and neap tides. Different water masses mix in the southern ECS, including the waters of the TS, ECS, and KC, to form a significant oceanic front. Strong horizontal convergence and vertical movement are expected to occur adjacent to the oceanic front in the southern ECS, inducing unstable ocean currents and a multiscale phenomenon. Considering the results from February 21 to 22, 2017 as an example, at this time, all four drifters flowed to the southern ECS (Figure 14). Figure 14a presents the hourly CODAR surface currents; these data reveal the high-frequency tidal excursion during flood and ebb cycles. The daily GHRSST on 21 February superimposed with the four drifter trajectories during 21–22 February is presented in Figure 14b. We used the drifting position of each drifter at 00:00 on 21 February and the hourly CODAR flow field to simulate the virtual drifter trajectory (the green line in Figure 14b). It is worth noting that the trajectories of the SVP drifters represented a 15 m depth ocean flow, while the trajectories of the virtual drifters were a near-surface flow. As shown in Figure 14b, Drifter-2 has a high degree of agreement with the virtual drifter, and the directions of Drifter-3 and Drifter-4 were similar; only Drifter-1 significantly differed from the virtual drifter. The spatial distribution of the flow field off northeastern Taiwan is closely related to the local submarine topography, and it is found that the KC branch could flow through the submarine canyon and cross the steep shelf edge into the ECS shelf (Tang & Yang, 1993; Tang et al., 1999, 2000). The ocean currents in this region include surface currents closely related to wind, the subsurface waters of the KC uplifted by topography (Liu et al., 1992), and the regurgitation of the KC in the bottom layer (Chuang et al., 1993). Therefore, the trajectories of the virtual drifters were slightly different from those of the SVP drifters. The strong KC intrusion around the region of 25.8°N caused the flow structures of the far and near shores to be different. The nearshore flow field even displayed a reverse flow (opposite to the direction of the

10.1029/2021JC017373

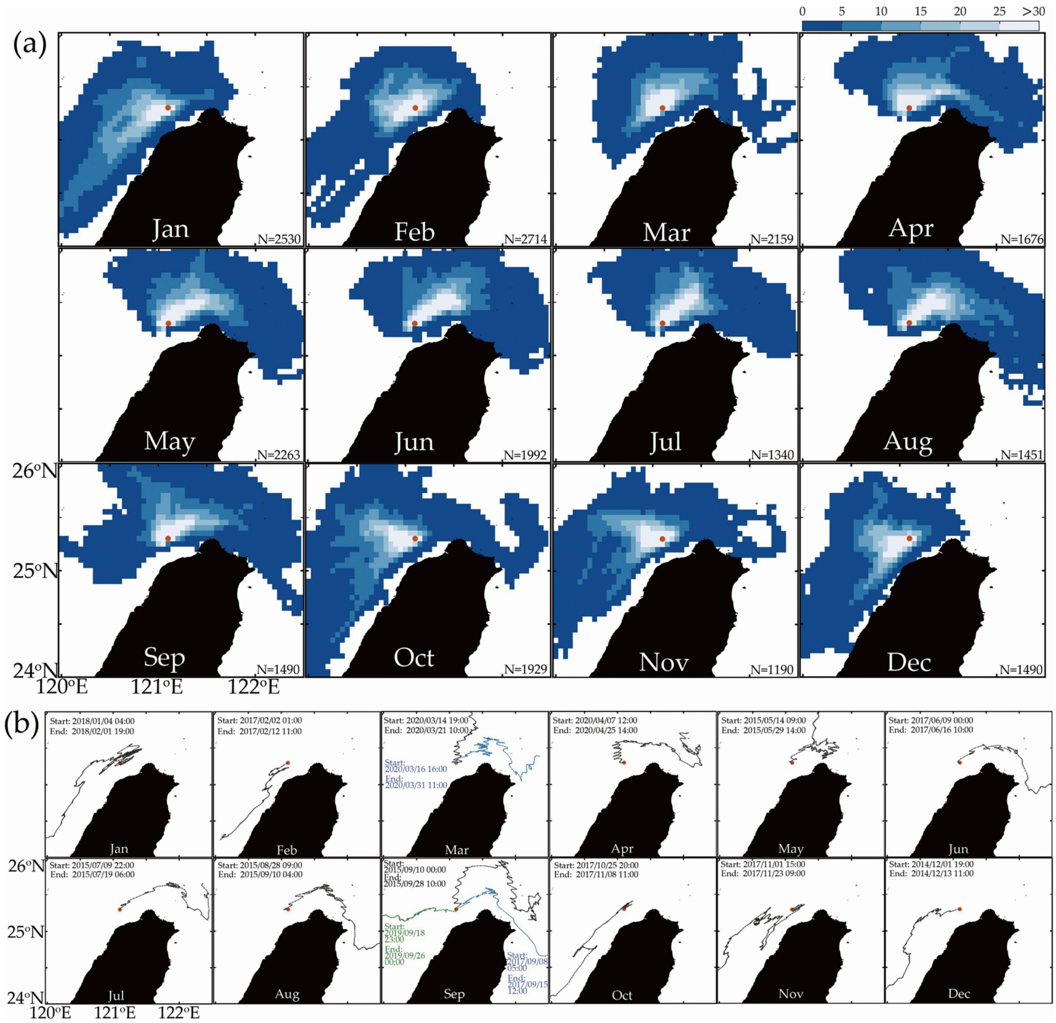

Figure 15. (a) The probability distribution of the virtual drifter trajectory in each month, where the red dot is the deployed position of the virtual drifter (121.1°E, 25.3°N), and the background color is the probability (%). (b) Examples of virtual drifter trajectories in each month.

KC), and the spatial structure of the oceanic front was significantly different in this region. The time span of the SVP drifter experiment was between February and March, when the northeasterly monsoon prevails in northern Taiwan with an average wind speed of 8–10 m/s. Although a small amount of wind-driven current was produced, the effect of wind on the trajectories of the SVP drifters was limited. The flow velocities of the drifters were obviously affected by the flood and ebb tidal currents, causing the trajectories to periodically swing back and forth and moving the drifters along the low-frequency flow.

2.7. Virtual Drifter Experiments Based on the Hourly CODAR Flow Field

In the previous section, we explored the results of the movement trajectories of four drifters, indicating clear variations in the tidal currents. To further explore the surface flow-field structure in the southern ECS, we conducted a virtual drifter experiment based on the hourly CODAR flow field. The release position of the virtual drifter was at 121.1°E, 25.3°N (marked as a red dot in Figure 15a), located at the junction of the TS and the southern ECS. The virtual drifter was continuously deployed from December 2014 to May 2020 at an interval of 1 hr. It is worth noting that data quality can limit the CODAR flow field, resulting in some missing data in relation to times and positions. For the purposes of this experiment, we therefore only selected data when the drifter had drifted continuously for >48 hr. We made a monthly probability density distribution chart of the drifter trajectories (Figure 15a). Arbitrary examples of near-surface drifting were chosen for each month but for different years from the virtual drifter experiments (Figure 15b), which last for a long time and can best represent the typical trajectory of the month. The drifter trajectory distribution for each month shown in Figure 15a agrees with the conceptual map of the flow-field characteristics in the southern ECS shown in Figure 6. June to August constitutes the typical summer period, during which most of the drifters flowed into the ECS or entered the KC along the northern coast of Taiwan. This outcome confirmed the findings of previous studies that used long-term observations to determine whether the water of the bay in northeastern Taiwan has the characteristics of summer ECS water masses (Hsu et al., 2018). In September, during the seasonal transition, we found that the drifter trajectories displayed three divergences: a northwestward flow toward the ECS, a northeastward flow toward the coast of Taiwan, and a southwestward flow toward the entrance of the TS. In October, the main distribution of the drifter trajectory changed to a southwestward flow entering the TS. This flow-field characteristic, known as the NTCC (as shown in Figure 6), continued until January. The drifter distributions in February and March once again showed a seasonal transition period. At the junction of the TS and the ECS, the ocean surface current gradually changed from a southward to a northward current, continuing to the next surface current cycle. Regarding the individual virtual drifter trajectories (Figure 15b), the path characteristics were the same as those observed in the SVP drifter experiment. Both drifters could be affected by the currents and become trapped or break away from tidal current restrictions and follow the direction of the main seasonal currents.

2.8. Variations in Oceanic Fronts in the Southern ECS

By comparing the variation in the SST observed by the four SVP drifters shown in Figure 10 with the results shown in Figures 7 and 15, the physical mechanism that caused these drifters to flow at the southern end of the ECS for2 months can be understood more clearly. When these drifters were released on the northwest side of the TS, they followed the monthly ocean current during February and moved to the northern coast of Taiwan. After being affected by strong tidal currents for several days, the drifters escaped the areas significantly affected by tides and then entered the KC, which carried them northward in March. These SVP drifter experiments recorded the results as the drifters encountered the oceanic front, and the SSTs were observed to vary rapidly within short drift distances. In the 6 months from October to March, several changes occurred in the SST front in the southern ECS. We therefore used long-term SST, chlorophyll concentrations, and SSS data to explore the characteristic variations in the oceanic front (Figure 16). The period from October to March also showed a rapid water transition in the southern ECS. The KI pushed high-SST seawater westward from the KC side, and the CCC pushed low-SST seawater southward on the TS side. The low- and high-SST water masses converged at the junction of the TS and the southern ECS, and the SST isotherms in the southern ECS were generally denser than those in the TS (Figure 16a). The strongest position of the SST front lies at approximately 121.5°E in the southern ECS. From the perspective of the ocean dynamic structure, the interface produced by the intersection of two different ocean currents or water masses regularly becomes a water environment that forms a rich fishing ground, referred to as the boundary of mass fishing waters. Here, the SST and SSS gradients were large. From December to March, the SST frontal isotherms were dense. If the horizontal gradient of the SST distribution in the fishing ground increased, it would reduce the range of the fish's temperature-appropriate sea area and promote a dense distribution of fish. In addition, the different directions of ocean currents would also be expected to bring a variety of fish species. As shown in Figure 16b, the variations in chlorophyll concentration are driven by seasonal currents. From October, the low-nutrient surface KC flowed toward the TS, forming a significant chlorophyll front that was most evident in December and January. From February, the flow along the western coast of Taiwan changed from the NTCC to the TSC. It can thus be seen that a water mass in the TS produced a waterway with a slightly lower chlorophyll concentration. The high chlorophyll concentration observed along the northwestern coast of Taiwan was caused by the continuous injection of river water. The SSS observational data also identified a salinity front formed by the mixing of the high-salinity KC and the low-salinity nearshore waters (Figure 16c). From the above results, we suggest that the current changes in the southern ECS could cause important oceanic fronts, with the most significant position adjacent to 121°E–122°E. From March to September, the water in the TS was dominated by the TSC moving from south to north, bringing into the southern ECS waters with high SSTs, SSSs, and low chlorophyll concentrations. The oceanic front in the southern ECS was not as pronounced in the summer as in the winter. The monthly characteristics of the eastern waters of Taiwan in the summer presented high levels of SST and

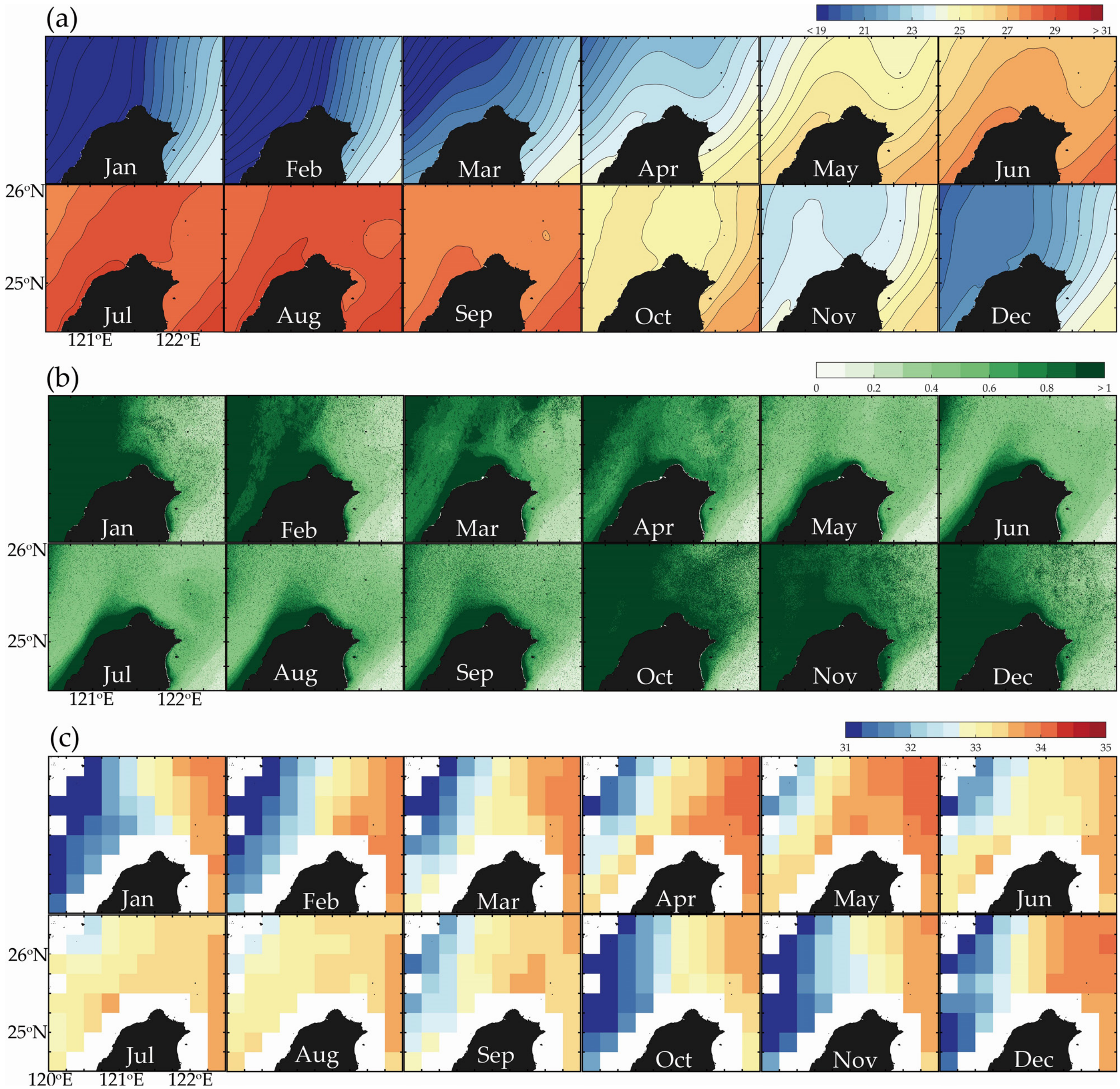

Figure 16. The long-term characteristics of the ocean parameters in each month in the southern ECS: (a) SST (°C) from June 2002 to October 2020; (b) chlorophyll concentration (mg/m^3) from April 2011 to October 2020; and (c) SSS (psu) from May 2015 to October 2020.

SSS seawater; however, the large amount of precipitation brought by a typhoon can cause short-term low SSTs and SSSs (Hsu & Ho, 2019). Moreover, the high chlorophyll concentration observed along the coast of Taiwan occurred due to river runoff.

3. Discussion and Conclusions

We speculate that, due to the scanning path and the limitation of the satellite altimeter along-track observations, which could only estimate results with low spatial and temporal resolutions, the satellite data might not be able to present the correct ocean surface current in the local area adjacent to the southern ECS. Wang and Oey (2016) observed that the on-shelf intrusion of drifters is significantly related to the winter onshore pattern of the KC path and that the warmer waters of the KC northeast of Taiwan produced a strong

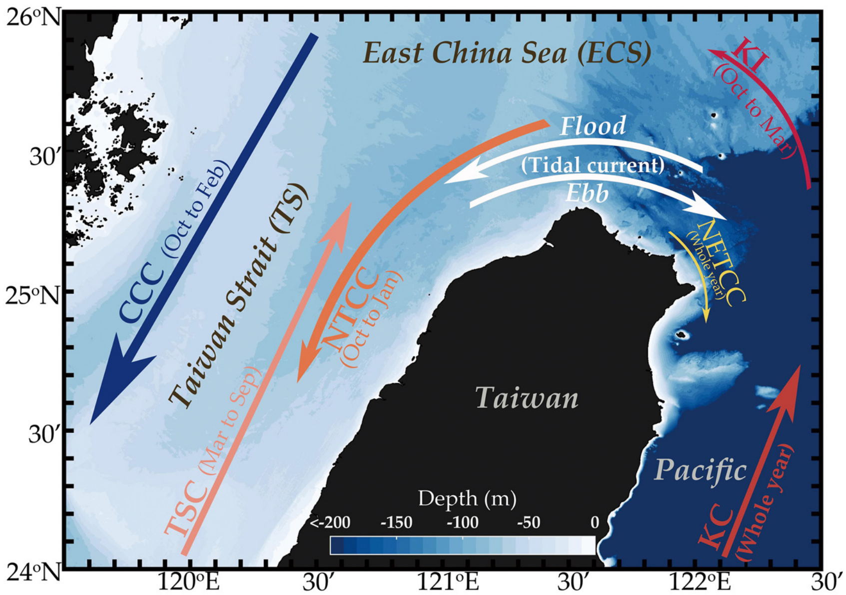

Figure 17. A schematic diagram of the main ocean surface currents in the southern ECS.

along-shelf sea level slope, resulting in a pressure gradient force that enabled the drifters to penetrate the prevailing monsoon wind. They also found that the strong KI is a result of potential vorticity constraints, and the current intrusion off northeastern Taiwan is the most important intrusion in the whole southern ECS. The analyses of CODAR long-term observations in this study confirmed that the KC intruded the ECS shelf and that the intruding water continued to flow westward to enter the TS before flowing southward with the northeasterly monsoon. We used this result to propose a current feature that appeared in the southern ECS in the winter: the NTCC (Figure 17). This result also confirmed the inference caused by the near-surface circulation in the southern ECS in the winter that Qiu et al. (2011) described based on 20 years of drifter data. The deployment of the four drifters at the junction of the TS and the southern ECS provided interesting and important results from the most chaotic location and month of the studied flow field. Both the SVP and virtual drifter experiments (Figures 9 and 15, respectively) could be regarded as the results of the total currents in the southern ECS. The flow field is composed of high-frequency tidal currents and low-frequency main circulation. We found that the drifters always moved along the pathway of low-frequency currents with high-frequency tidal signatures and cyclic movement patterns. Off northern Taiwan, the velocities of the total currents are weak due to the intersection of various currents in different directions all year. The white line segment in Figure 17 is used to emphasize the direction of the tidal current in northern Taiwan.

Regarding future work, ocean research surveys should be used to continuously measure the ocean currents and hydrological structures in this region. For example, the use of long-term hydrological survey data covering the summer months over the past 25 years allowed us to further understand the changes in the water layers of the entire upper seawater zone (100 m) at the junction of the oceanic fronts, including the front generated by the flow of the TSC, which passes northern Taiwan and deflects eastward in the summer and the upwelling caused by the cold dome off northeastern Taiwan. We expect that more cruise observations conducted in the winter will clarify the smaller-scale ocean phenomena, and it is necessary for researchers to establish in situ measurement cruises and long-term observations to understand the hydrological exchanges occurring off northern Taiwan in the future. Some issues on the east side of the TS are still worthy of further discussion, including the branching and eastward deflection mechanisms of the TSC at the northern end of the TS, the impacts of the sudden strengthening and expansion of the CCC on the TS, and the contributions of river runoff and the chlorophyll concentration along the northern coast of Taiwan to the southern ECS. In addition, studying oceanic front changes at an annual scale could also help to clarify the link between fishing grounds (Oey et al., 2018) and ocean physics.

In summary, this study aimed to explore the ocean surface currents and oceanic fronts in the southern ECS using a high-spatiotemporal-resolution CODAR flow field in conjunction with satellite data and the results of four SVP drifter experiments. Based on CODAR-mapped surface current, the dynamic mechanisms of surface waters in the southern ECS were discovered and confirmed. Beginning in October, an ocean current called the NTCC flows along the northwestern coast of Taiwan to the southwestern TS and can last until February, with a velocity of 0.1–0.2 m/s; the current is most significant in December. The NTCC and CCC constitute the surface flows in the northern TS in the winter. In other seasons, the surface current in the northern TS is mainly composed of the TSC (0.3–0.5 m/s). In February 2017, four drifters were deployed at the junction of the TS and southern ECS. On a monthly scale, the drifters' low-frequency movements were dominated by the seasonal current in the southern ECS, drifting from the TS to the northern coast of Taiwan and then to the KC. On a daily scale, the drifters' high-frequency movements were characterized by strong tidal currents that caused the trajectories to rotate and oscillate and caused the drifters to become trapped in the region off northern Taiwan. The tidal current velocities were observed to exceed 1.2 m/s. Three drifters crossed the oceanic front with the characteristics of tidal trajectories; i.e., they flowed back and forth between low- and high-SST areas, and the SST could change by 2.5°C within 500 m. The combined use of the CODAR flow field and long-term satellite data helped us to understand the ocean current movements and the mechanisms of oceanic front generation. In winter, the KI pushed water with high SSTs and SSSs and low chlorophyll concentrations from the KC region to the northern TS. The most pronounced oceanic front position in the winter was located between 121°E and 122°E in the southern ECS. The detection of this front location will aid future surveys in detecting submesoscale and small-scale phenomena in the area, especially since underwater observational data obtained in the winter remain limited. Based on the CODAR-mapped hourly surface current, the virtual drifter experiment helped us to understand not only the drifting trajectories of the surface currents but also the reference values of oil pollution drifting, shipwreck rescues, and water mass mixing processes. Overall, we successfully clarified the characteristics of the surface currents in the southern ECS, and the data will continue to be used in field surveys in the future.

Data Availability Statement

Satellite altimetry data are distributed through the Copernicus Marine and Environment Monitoring Service (https://marine.copernicus.eu/). The OSCAR ocean surface current reanalysis data are available through https://doi.org/10.5067/OSCAR-03D01. The numerical model outputs of current field data obtained from HYCOM+NCODA are available through https://www.hycom.org/. Four drifter experimental datasets are available through the global drifter program (https://www.aoml.noaa.gov/phod/gdp/index.php). The CODAR data are available through TOROS (https://www.tori.narl.org.tw/ETORI/eDefault.aspx). The historical ADCP data are available through the ODB of the Ministry of Science and Technology, Taiwan (http://www.odb.ntu.edu.tw/en/). The GHRSST data are available through NASA's physical oceanography distributed active archive center (https://doi.org/10.5067/GHGMR-4FJ04). SMAP salinities are available through remote sensing systems, sponsored by NASA (https://doi.org/10.5067/SMP40-3SMCS). The GOCI data are available through the NASA ocean color web (https://doi.org/10.5067/COMS/GOCI/L2/OC/2014). The C-2015 ASCAT data are produced by remote sensing systems and sponsored by the NASA Ocean Vector Winds Science Team. Data are available at www.remss.com.

Acknowledgments
The authors appreciate all of the data provided from each open database. The authors thank the anonymous reviewers and journal editors for their comments. This work was supported by the Ministry of Science and Technology of Taiwan through Grants MOST 109-2611-M-110-018 and MOST 109-2811-M-019-502.

References

Barrick, D. E., Evans, M. W., & Weber, B. L. (1977). Ocean surface currents mapped by radar. *Science*, *198*(4313), 138–144. https://doi.org/10.1126/science.198.4313.138

Centurioni, L. R. (2018). Drifter technology and impacts for sea surface temperature, sea-level pressure, and ocean circulation studies. *In observing the oceans in real time* (pp. 37–57). Cham: Springer. https://doi.org/10.1007/978-3-319-66493-4_3

Chang, Y., Shimada, T., Lee, M. A., Lu, H. J., Sakaida, F., & Kawamura, H. (2006). Wintertime sea surface temperature fronts in the Taiwan Strait. *Geophysical Research Letters*, *33*(23). https://doi.org/10.1029/2006GL027415

Chen, C. T. A. (2008). Distributions of nutrients in the East China Sea and the South China Sea connection. *Journal of Oceanography*, *64*(5), 737–751. https://doi.org/10.1007/s10872-008-0062-9

Chen, C. T. A., & Sheu, D. D. (2006). Does the Taiwan warm current originate in the Taiwan strait in wintertime? *Journal of Geophysical Research*, *111*(C4). https://doi.org/10.1029/2005JC003281

Cheng, Y. H., Ho, C. R., Zheng, Z. W., Lee, Y. H., & Kuo, N. J. (2009). An algorithm for cold patch detection in the sea off northeast Taiwan using multi-sensor data. *Sensors*, *9*, 5521–5533. https://doi.org/10.3390/s90705521

Chuang, W. S., Li, H. W., Tang, T. Y., & Wu, C. K. (1993). Observations of the countercurrent on the inshore side of the Kuroshio northeast of Taiwan. *Journal of Oceanography*, *49*(5), 581–592. https://doi.org/10.1007/BF02237464

He, Y., Hu, P., Yin, Y., Liu, Z., Liu, Y., Hou, Y., & Zhang, Y. (2019). Vertical migration of the Along-Slope Counter-Flow and its relation with the Kuroshio intrusion off northeastern Taiwan. *Remote Sensing*, *11*(22), 2624. https://doi.org/10.3390/rs11222624

Hsin, Y. C., Chiang, T. L., & Wu, C. R. (2011). Fluctuations of the thermal fronts off northeastern Taiwan. *Journal of Geophysical Research*, *116*(C10). https://doi.org/10.1029/2011JC007066

Hsu, P. C. & Ho, C. R. (2019). Typhoon-induced ocean subsurface variations from glider data in the Kuroshio region adjacent to Taiwan. *Journal of Oceanography*, *75*(1), 1–21. https://doi.org/10.1007/s10872-018-0480-2

Hsu, P. C., Lu, C. Y., Hsu, T. W., & Ho, C. R. (2020). Diurnal to seasonal variations in ocean chlorophyll and ocean currents in the north of Taiwan observed by geostationary ocean color imager and coastal radar. *Remote Sensing*, *12*(17), 2853. https://doi.org/10.3390/rs12172853

Hsu, P. C., Zheng, Q., Lu, C. Y., Cheng, K. H., Lee, H. J., & Ho, C. R. (2018). Interaction of coastal countercurrent in I-Lan Bay with the Kuroshio northeast of Taiwan. *Continental Shelf Research*, *171*, 30–41. https://doi.org/10.1016/j.csr.2018.10.012

Hu, F., Liu, Y., Xu, Z., Yin, Y., & Hou, Y. (2020). Bidirectional volume exchange between Kuroshio and East China Sea Shelf Water based on a whole-region passive-tracing method. *Journal of Geophysical Research: Oceans*, *125*(5), e2019JC015528. https://doi.org/10.1029/2019JC015528

Hu, J., Kawamura, H., Li, C., Hong, H., & Jiang, Y. (2010). Review on current and seawater volume transport through the Taiwan Strait. *Journal of Oceanography*, *66*(5), 591–610. https://doi.org/10.1007/s10872-010-0049-1

Jan, S., Chen, C. C., Tsai, Y. L., Yang, Y. J., Wang, J., Chern, C. S., et al. (2011). Mean structure and variability of the cold dome northeast of Taiwan. *Oceanography*, *24*(4), 100–109. https://doi.org/10.5670/oceanog.2011.98

Jan, S., Chern, C. S., & Wang, J. (2002). Transition of tidal waves from the East to South China Seas over the Taiwan Strait: Influence of the abrupt step in the topography. *Journal of Oceanography*, *58*(6), 837–850. https://doi.org/10.1023/A:1022827330693

Jan, S., Chern, C. S., Wang, J., & Chao, S. Y. (2004). The anomalous amplification of M2 tide in the Taiwan Strait. *Geophysical Research Letters*, *31*(7). https://doi.org/10.1029/2003GL019373

Jan, S., Tseng, Y. H., & Dietrich, D. E. (2010). Sources of water in the Taiwan Strait. *Journal of Oceanography*, *66*(2), 211–221. https://doi.org/10.1007/s10872-010-0019-7

Jan, S., Wang, J., Chern, C. S., & Chao, S. Y. (2002). Seasonal variation of the circulation in the Taiwan Strait. *Journal of Marine Systems*, *35*(3-4), 249–268. https://doi.org/10.1016/S0924-7963(02)00130-6

Ko, D. S., Preller, R. H., Jacobs, G. A., Tang, T. Y., & Lin, S. F. (2003). Transport reversals at Taiwan strait during October and November 1999. *Journal of Geophysical Research: Oceans*, *108*(C11). https://doi.org/10.1029/2003JC001836

Liao, E., Yan, X. H., & Jiang, Y. (2017). The role of coastal-trapped waves on the 2008 cold disaster in the Taiwan Strait. *Ocean Dynamics*, *67*(5), 611–619. https://doi.org/10.1007/s10236-017-1042-7

Lie, H. J., & Cho, C. H. (2016). Seasonal circulation patterns of the Yellow and East China Seas derived from satellite-tracked drifter trajectories and hydrographic observations. *Progress in Oceanography*, *146*, 121–141. https://doi.org/10.1016/j.pocean.2016.06.004

Lin, X., Yan, X. H., Jiang, Y., & Zhang, Z. (2016). Performance assessment for an operational ocean model of the Taiwan Strait. *Ocean Modelling*, *102*, 27–44. https://doi.org/10.1016/j.ocemod.2016.04.006

Lipa, B., Nyden, B., Ullman, D. S., & Terrill, E. (2006). SeaSonde radial velocities: Derivation and internal consistency. *IEEE Journal of Oceanic Engineering*, *31*(4), 850–861. https://doi.org/10.1109/JOE.2006.886104

Liu, K. K., Gong, G. C., Lin, S., Yang, C. Y., Wei, C. L., Pai, S. C., & Wu, C. K. (1992). The year-round upwelling at the shelf break near the northern tip of Taiwan as evidenced by chemical hydrography. *Terrestrial, Atmospheric and Oceanic Sciences*, *3*(3), 243–275. https://doi.org/10.3319/tao.1992.3.3.243(keep)

Liu, K. K., Tang, T. Y., Gong, G. C., Chen, L. Y., & Shiah, F. K. (2000). Cross-shelf and along-shelf nutrient fluxes derived from flow fields and chemical hydrography observed in the southern East China Sea off northern Taiwan. *Continental Shelf Research*, *20*(4-5), 493–523. https://doi.org/10.1016/S0278-4343(99)00083-7

Liu, X., Dong, C., Chen, D., & Su, J. (2014). The pattern and variability of winter Kuroshio intrusion northeast of Taiwan. *Journal of Geophysical Research: Oceans*, *119*(8), 5380–5394. https://doi.org/10.1002/2014JC009879

Liu, X., Wang, D. P., Su, J., Chen, D., Lian, T., Dong, C., & Liu, T. (2020). On the vorticity balance over steep slopes: Kuroshio intrusions northeast of Taiwan. *Journal of Physical Oceanography*, *50*(8), 2089–2104. https://doi.org/10.1175/JPO-D-19-0272.1

Naimullah, M., Lan, K. W., Liao, C. H., Hsiao, P. Y., Liang, Y. R., & Chiu, T. C. (2020). Association of environmental factors in the Taiwan Strait with distributions and habitat characteristics of three swimming crabs. *Remote Sensing*, *12*(14), 2231. https://doi.org/10.3390/rs12142231

Oey, L. Y., Hsin, Y. C., & Wu, C. R. (2010). Why does the Kuroshio northeast of Taiwan shift shelfward in winter? *Ocean Dynamics*, *60*(2), 413–426. https://doi.org/10.1007/s10236-009-0259-5

Oey, L. Y., Wang, J., & Lee, M. A. (2018). Fish catch is related to the fluctuations of a western boundary current. *Journal of Physical Oceanography*, *48*(3), 705–721. https://doi.org/10.1175/JPO-D-17-0041.1

Qiu, Y., Li, L., Chen, C. T. A., Guo, X., & Jing, C. (2011). Currents in the Taiwan Strait as observed by surface drifters. *Journal of Oceanography*, *67*(4), 395–404. https://doi.org/10.1007/s10872-011-0033-4

Roarty, H., Cook, T., Hazard, L., George, D., Harlan, J., Cosoli, S., et al. (2019). The global high frequency radar network. *Frontiers in Marine Science*, *6*, 164. https://doi.org/10.3389/fmars.2019.00164

Shen, Y. T., Lai, J. W., Leu, L. G., Lu, Y. C., Chen, J. M., Shao, H. J., & Tseng, R. S. (2019). Applications of ocean currents data from high-frequency radars and current profilers to search and rescue missions around Taiwan. *Journal of Operational Oceanography*, *12*(sup. 2), S126–S136. https://doi.org/10.1080/1755876X.2018.1541538

Tang, T. Y., Hsueh, Y., Yang, Y. J., & Ma, J. C. (1999). Continental slope flow northeast of Taiwan. *Journal of Physical Oceanography*, *29*(6), 1353–1362. https://doi.org/10.1175/1520-0485(1999)029<1353:csfnot>2.0.co;2

Tang, T. Y., Tai, J. H., & Yang, Y. J. (2000). The flow pattern north of Taiwan and the migration of the Kuroshio. *Continental Shelf Research*, *20*(4-5), 349–371. https://doi.org/10.1016/S0278-4343(99)00076-X

Tang, T. Y., & Yang, Y. J. (1993). Low frequency current variability on the shelf break northeast of Taiwan. *Journal of Oceanography*, *49*(2), 193–210. https://doi.org/10.1007/BF02237288

Tseng, R.-S., & Shen, Y.-T. (2003). Lagrangian observations of surface flow patterns in the vicinity of Taiwan. *Deep-Sea Research II*, *50*(6-7), 1107–1115. https://doi.org/10.1016/S0967-0645(03)00012-2

Wang, J., & Oey, L. Y. (2016). Seasonal exchanges of the Kuroshio and shelf waters and their impacts on the shelf currents of the East China Sea. *Journal of Physical Oceanography*, *46*(5), 1615–1632. https://doi.org/10.1175/JPO-D-15-0183.1

Wu, C. R., Chao, S. Y., & Hsu, C. (2007). Transient, seasonal and interannual variability of the Taiwan Strait current. *Journal of Oceanography*, *63*(5), 821–833. https://doi.org/10.1007/s10872-007-0070-1

Wu, C. R., Lu, H. F., & Chao, S. Y. (2008). A numerical study on the formation of upwelling off northeast Taiwan. *Journal of Geophysical Research: Oceans*, *113*(C8). https://doi.org/10.1029/2007JC004697

Yin, Y., Liu, Z., Hu, P., Hou, Y., Lu, J., & He, Y. (2020). Impact of mesoscale eddies on the southwestward countercurrent northeast of Taiwan revealed by ADCP mooring observations. *Continental Shelf Research*, *195*, 104063. https://doi.org/10.1016/j.csr.2020.104063

Yu, J. C. S., Chou, T. Y., Yu, H. C., Chen, P., Vanhellemont, Q., & Fettweis, M. (2016). Surface suspended particulate matter concentration in the Taiwan Strait during summer and winter monsoons. *Ocean Dynamics*, *66*(11), 1517–1527. https://doi.org/10.1007/s10236-016-0992-5

Zhang, C., Huang, Y., & Ding, W. (2020). Enhancement of Zhe-Min coastal water in the Taiwan Strait in winter. *Journal of Oceanography*, *76*, 197–209. https://doi.org/10.1007/s10872-020-00539-5

Zhou, P., Song, X., Yuan, Y., Cao, X., Wang, W., Chi, L., & Yu, Z. (2018). Water mass analysis of the East China Sea and interannual variation of Kuroshio subsurface water intrusion through an optimum multiparameter method. *Journal of Geophysical Research: Oceans*, *123*(5), 3723–3738. https://doi.org/10.1029/2018JC013882

Zhuang, Z., Zheng, Q., Zhang, X., Yang, G., Zhao, X., Cao, L., et al. (2020). Variability of Kuroshio surface axis northeast of Taiwan island derived from satellite altimeter data. *Remote Sensing*, *12*(7), 1059. https://doi.org/10.3390/rs12071059